



**HAL**  
open science

## Reassessment of the phylogenetic relationships of the late Miocene apes *Hispanopithecus* and *Rudapithecus* based on vestibular morphology

Alessandro Urciuoli, Clément Zanolli, Sergio Almécija, Amélie Beaudet, Jean Dumoncel, Naoki Morimoto, Nakatsukasa Masato, Salvador Moyà-Solà, David R. Begun, David Alba

### ► To cite this version:

Alessandro Urciuoli, Clément Zanolli, Sergio Almécija, Amélie Beaudet, Jean Dumoncel, et al.. Re-assessment of the phylogenetic relationships of the late Miocene apes *Hispanopithecus* and *Rudapithecus* based on vestibular morphology. *Proceedings of the National Academy of Sciences of the United States of America*, 2021, 118 (5), pp.e2015215118. 10.1073/pnas.2015215118. hal-03152572

**HAL Id: hal-03152572**

**<https://hal.science/hal-03152572>**

Submitted on 25 Feb 2021

**HAL** is a multi-disciplinary open access archive for the deposit and dissemination of scientific research documents, whether they are published or not. The documents may come from teaching and research institutions in France or abroad, or from public or private research centers.

L'archive ouverte pluridisciplinaire **HAL**, est destinée au dépôt et à la diffusion de documents scientifiques de niveau recherche, publiés ou non, émanant des établissements d'enseignement et de recherche français ou étrangers, des laboratoires publics ou privés.

1 BIOLOGICAL SCIENCES: Anthropology

2

3 **Reassessment of the phylogenetic relationships of the late Miocene apes**

4 ***Hispanopithecus* and *Rudapithecus* based on vestibular morphology**

5

6 Alessandro Urciuoli<sup>a,\*</sup>, Clément Zanolli<sup>b</sup>, Sergio Almécija<sup>c,d,a</sup>, Amélie Beaudet<sup>e,f</sup>, Jean

7 Dumoncel<sup>g</sup>, Naoki Morimoto<sup>h</sup>, Masato Nakatsukasa<sup>h</sup>, Salvador Moyà-Solà<sup>a,i,j</sup>, David

8 R. Begun<sup>k</sup>, David M. Alba<sup>a,\*</sup>

9

10 <sup>a</sup>Institut Català de Paleontologia Miquel Crusafont, Universitat Autònoma de

11 Barcelona, Edifici ICTA-ICP, c/ Columnes s/n, Campus de la UAB, 08193

12 Cerdanyola del Vallès, Barcelona, Spain; <sup>b</sup>*Univ. Bordeaux, CNRS, MCC, PACEA,*

13 *UMR 5199, F-33600 Pessac, France;* <sup>c</sup>Division of Anthropology, American Museum

14 of Natural History, Central Park West at 79th Street, New York, NY 10024, USA;

15 <sup>d</sup>New York Consortium in Evolutionary Primatology, New York, USA; <sup>e</sup>School of

16 Geography, Archaeology and Environmental Studies, University of the

17 Witwatersrand, Private Bag 3, Johannesburg, WITS 2050, South Africa; <sup>f</sup>Department

18 of Anatomy, University of Pretoria, PO Box 2034, Pretoria, 0001, South Africa;

19 <sup>g</sup>Laboratoire AMIS, UMR 5288 CNRS, Université de Toulouse, Allées Jules Guesde

20 37, 31073, Toulouse, France; <sup>h</sup>Laboratory of Physical Anthropology, Graduate

21 School of Science, Kyoto University, Kyoto, 606 8502, Japan; <sup>i</sup>Institució Catalana de

22 Recerca i Estudis Avançats (ICREA), Passeig de Lluís Companys 23, 08010

23 Barcelona, Spain; <sup>j</sup>Unitat d'Antropologia (Departament de Biologia Animal, Biologia

24 Vegetal i Ecologia), Universitat Autònoma de Barcelona, Campus de la UAB s/n,

25 08193 Cerdanyola del Vallès, Barcelona, Spain; <sup>k</sup>Department of Anthropology,

26 University of Toronto, Toronto, ON M5S 2S2, Canada

27

28 \*To whom correspondence should be addressed:

29

30 Alessandro Urciuoli

31 Postal address: Institut Català de Paleontologia Miquel Crusafont, Universitat  
32 Autònoma de Barcelona, Edifici ICTA-ICP, c/ Columnes s/n, Campus de la UAB,  
33 08193 Cerdanyola del Vallès, Barcelona, Spain

34 Phone: +34 622112509

35 Email: [alessandro.urciuoli@icp.cat](mailto:alessandro.urciuoli@icp.cat)

36

37 David M. Alba

38 Postal address: Institut Català de Paleontologia Miquel Crusafont, Universitat  
39 Autònoma de Barcelona, Edifici ICTA-ICP, c/ Columnes s/n, Campus de la UAB,  
40 08193 Cerdanyola del Vallès, Barcelona, Spain

41 Phone: +34 935868604

42 Email: david.alba@icp.cat

43

44 **Keywords:** inner ear, semicircular canals, evolution, fossil apes, Hominidae.

45

46 ORCID:

47 Alessandro Urciuoli: 0000-0002-6265-8962

48 Clément Zanolli: 0000-0002-5617-1613

49 Sergio Almécija: 0000-0003-1373-1497

50 Amélie Beaudet: 0000-0002-9363-5966

51 Jean Dumoncel: 0000-0003-0789-7458

52 Naoki Morimoto: 0000-0002-8367-4777

53 Masato Nakatsukasa: 0000-0002-6897-8027

54 Salvador Moyà-Solà: 0000-0001-8506-1061

55 David R. Begun: 0000-0001-8916-6442

56 David M. Alba: 0000-0002-8886-5580

57

58

59 **Abstract**

60 **Late Miocene great apes are key to reconstructing the ancestral morphotype**  
61 **from which earliest hominins evolved. Despite consensus that the late**  
62 **Miocene dryopith great apes *Hispanopithecus laietanus* (Spain) and**  
63 ***Rudapithecus hungaricus* (Hungary) are closely related (Hominidae), ongoing**  
64 **debate on their phylogenetic relationships with extant apes (stem hominids,**  
65 **hominines, or pongines) complicates our understanding of great ape and**  
66 **human evolution. To clarify this question, we rely on the morphology of the**  
67 **inner ear semicircular canals, which has been shown to be phylogenetically**  
68 **informative. Based on microcomputed tomography scans, we describe the**  
69 **vestibular morphology of *Hispanopithecus* and *Rudapithecus*, and compare**  
70 **them with extant hominoids using landmark-free deformation-based 3D**  
71 **geometric morphometric analyses. We also provide critical evidence about the**  
72 **evolutionary patterns of the vestibular apparatus in living and fossil hominoids**  
73 **under different phylogenetic assumptions for dryopiths. Our results are**  
74 **consistent with the distinction of *Rudapithecus* and *Hispanopithecus* at the**  
75 **genus rank, and further support their allocation to the Hominidae based on**  
76 **their derived semicircular canal volumetric proportions. Compared with extant**  
77 **hominids, the vestibular morphology of *Hispanopithecus* and *Rudapithecus***  
78 **most closely resembles that of African apes, and differs from the derived**  
79 **condition of orangutans. However, the vestibular morphologies reconstructed**  
80 **for the last common ancestors of dryopiths, crown hominines, and crown**  
81 **hominids are very similar, indicating that hominines are plesiomorphic in this**  
82 **regard. Therefore, our results do not conclusively favor a hominine or stem**  
83 **hominid status for the investigated dryopiths.**

84

85 **Significance**

86       Reconstructing the phylogenetic relationships of extinct apes is challenging due to  
87 their fragmentary fossil record and the recurrent independent evolution of  
88 morphological features. Given the relevance of the phylogenetic signal of the bony  
89 labyrinth, here we assess the phylogenetic affinities of the late Miocene great apes  
90 *Hispanopithecus* and *Rudapithecus* by studying their inner ear morphology. Our  
91 results are consistent with the distinct generic status of these dryopiths, which further  
92 differ from the derived condition of orangutans and most closely resemble African  
93 apes. However, the latter appear largely primitive (similar to the last common  
94 ancestor of great apes and humans), hence our results do not conclusively favor a  
95 closer relationship with African apes as opposed to great apes as a whole.

96

97

98 Hominoids (apes and humans) originated in Africa during the Oligocene (1) but  
99 subsequently dispersed into Eurasia, giving rise to an impressive radiation during the  
100 middle and late Miocene (2-3). Thus, while extant hominoids include only two  
101 moderately diverse families—hylobatids (gibbons and siamangs) and hominids  
102 (great apes and humans)—the panoply of extinct genera recorded during the  
103 Miocene still defies classification into a coherent systematic scheme. Other than the  
104 late Miocene *Oreopithecus*—which might be a late occurring stem hominoid (4, 5) —  
105 there is consensus that most Eurasian large-bodied hominoids are members of the  
106 great-ape-and-human clade (Hominidae) (2, 3, 6). While most Asian extinct great  
107 apes such as *Sivapithecus* are considered to be more closely related to the  
108 orangutan clade (Ponginae) than to African apes and humans (Homininae) (2, 6-8),  
109 the phylogenetic affinities of European *Dryopithecus* and allied forms have long been  
110 debated. Until a decade ago, several species of European apes from the middle and  
111 late Miocene were included within this genus (9-16). However, discoveries at the  
112 middle Miocene composite section of Abocador de Can Mata (6, 17-20) prompted  
113 the recognition that the late Miocene species belong to one or more different genera  
114 distinct from/other than *Dryopithecus* (2-3, 6, 7, 18, 21-26): *Hispanopithecus* from  
115 Spain, and *Rudapithecus* from Hungary, the latter formerly considered a subgenus of  
116 the former by some authors (6, 18, 22).

117 Together with *Dryopithecus* and other middle to late Miocene taxa (17, 19, 27),  
118 *Hispanopithecus* and *Rudapithecus* are currently classified in a subfamily  
119 (Dryopithecinae) (6, 20, 26) or tribe (Dryopithecini) (3, 7, 21) of their own, distinct  
120 from pongines. Both taxa possess a hominid-like cranial morphology (6, 11-13, 21,  
121 25, 29-30), as shown by the high zygomatic root, reduced midfacial prognathism,  
122 lack of subarcuate fossa, deep glenoid fossa, and prominent entoglenoid process.

123 However, there is no consensus regarding the phylogenetic position of this group—  
124 being either considered stem hominids (6, 19, 28), stem hominines (2-3, 14, 16, 25),  
125 or even pongines (10, 29-30) —which may be informally referred to as ‘dryopiths’.  
126 Resolving the phylogenetic position of dryopiths has important implications for the  
127 evolution of the great ape and human clade, since their purported hominine status  
128 has led to paleobiogeographic scenarios favoring a European origin and subsequent  
129 back-to-Africa dispersal for the African and human clade (2-3, 15, 24-25).  
130 Disagreements and uncertainties about the phylogenetic position of extinct apes are  
131 persistent, and stem from a combination of factors, including the incomplete and  
132 fragmentary hominoid fossil record, the decimated current diversity of the group, and  
133 pervasive homoplasy coupled with mosaic evolution (6, 23, 31-35).

134 The morphology of the semicircular canals (SCs), which partly constitute the inner  
135 ear’s bony labyrinth, has been classically related to locomotion (36-42). However,  
136 several studies have highlighted the possibility of inferring phylogenetic relatedness  
137 based on this portion of the inner ear morphology (43-47) Recently, it has been  
138 shown that this anatomical structure also embeds a strong phylogenetic signal  
139 among catarrhine primates by means of 3D geometric morphometric (3DGM)  
140 analyses (5, 47-49), thus being potentially useful to test phylogenetic hypotheses for  
141 extinct hominoids. Previous studies relied on the SC radius of *Rudapithecus*  
142 *hungaricus* and *Hispanopithecus laietanus* to infer slow and deliberate arboreal  
143 locomotion for these species (41). However, recent analyses raised doubts about the  
144 reliability of locomotor behavior predictions based on SC radius only (50-51). In  
145 contrast, here we rely on  $\mu$ CT scans of the same specimens and a deformation-  
146 based (landmark-free) 3DGM approach to assess their closest affinities in SC  
147 morphology with extant hominoids and interpret them from an evolutionary viewpoint.

148 First, we describe the fossil remains and qualitatively compare them with extant  
149 hominoids. Second, we assess if the volumetric proportions of their SCs more  
150 closely resemble those of hominids than those of other anthropoids. Third, we  
151 quantitatively evaluate changes in SC and vestibule morphology by means of a  
152 between-group principal component analysis (bgPCA) applied to a sample of extant  
153 and extinct hominoids. The affinities of the investigated fossil taxa are further  
154 assessed by means of cluster analyses and group membership probabilities based  
155 bgPCA results. Finally, we reconstruct the evolutionary history of the hominoid SCs  
156 using a phylomorphospace approach (including reconstructed ancestral  
157 morphotypes) under various phylogenetic assumptions for dryopiths.

158

## 159 **Results**

160 **Descriptions and comparisons.** Three-dimensional renderings of the vestibular  
161 apparatus of fossil and extant hominoids investigated here are illustrated in the  
162 Figure 1a-m. The vestibular apparatus of *R. hungaricus* is well preserved in the three  
163 available specimens (Fig. 1a-c). As in extant hominids, the SCs are stout—although  
164 less so than in orangutans (Fig. 1j), most humans (Fig. 1m) and gorillas (Fig. 1k)—  
165 and the vestibule is large relative to the volume occupied by SCs. The anterior and  
166 posterior canals are large and similar in size (Fig. 1a,b). The anterior canal is slightly  
167 vertically compressed, as in extant hominoids and the fossil apes *Nyanzapithecus*  
168 *alesi* (4) and *Nacholapithecus kerioi* (Fig. 1f), and somewhat larger in RUD 77 than  
169 in RUD 200. The anterior canal is somewhat anterosuperiorly projecting, albeit much  
170 less so than in *Pongo* (Fig. 1j) and *Oreopithecus* (Fig. 1e). The lateral and posterior  
171 canals are slightly different between the two individuals. In RUD 77, the lateral canal  
172 is noticeably smaller than the other SCs (Fig. 1a,b), slightly compressed horizontally,



173 and slenderer than in RUD 200. The lateral canal of RUD 200 is stout and large,  
174 almost reaching the size of the vertical SCs (similar to the condition in African apes,  
175 yet smaller than in gorillas; Fig. 1c), and its slender portion connects with the  
176 vestibule somewhat more inferiorly than in RUD 77. The junction of the slender  
177 portion of the lateral canal and the ampulla further differs between the two  
178 individuals, as it protrudes anteriorly in RUD 200, while it is posterolaterally oriented  
179 in RUD 77. In both individuals, the ampullary portion bends superiorly and the  
180 slender segment between the connection with the vestibule and the posterolateral tip  
181 of the lateral canal is straight, as in *Hoolock* (Fig. 1g) and in most hominids (Fig. 1j-  
182 m)—except for some *Gorilla* and *Pan* specimens that show some curvature.  
183 However, this section of the canal is more laterally oriented in RUD 77, while it is  
184 almost parallel to the posterior canal in RUD 200. The posterior canal is elongated  
185 posterolaterally in RUD 77, as in gorillas (Fig. 1k) and some humans (Fig. 1m), while  
186 it is slightly more rounded in RUD 200 (Fig. 1c). In both RUD 77 and RUD 200, the  
187 posterior and lateral canals approximately define a right angle (slightly more obtuse  
188 in RUD 77) and the trajectory of the lateral canal does not intersect the plane  
189 identified by the posterior canal. The common crus (CC) is short and slender, with  
190 the slender portions of the anterior and posterior canals almost forming right angle at  
191 the CC apex. The SCs are almost coplanar, with a slight amount of torsion in the  
192 upper portion of the anterior one (the tip slightly bending medially), in the medial-  
193 most part of the posterior one (displaced anteriorly), and in the tip of the lateral canal  
194 (pointing inferiorly).

195 The vestibular apparatus of *H. laietanus* (Fig. 1d) differs from that of *Rudapithecus*  
196 (especially RUD 77; Fig. 1a,b) by being more voluminous and displaying more  
197 equally developed SCs. The larger volume is particularly appreciable on the

198 vestibular recesses (which are more voluminous than the SCs, as in orangutans; Fig.  
199 1j) and in the much more inflated ampullae. The anterior canal is more vertically  
200 compressed than in *Rudapithecus*, showing an almost rectangular shape. This canal  
201 is also much slenderer than in orangutans (Fig. 1j) and gorillas (Fig. 1k), most  
202 closely resembling chimpanzees (Fig. 1l). The lateral canal is stouter than the others,  
203 especially in the ampullary portion. Its posterolateral-most tip slightly bends inferiorly,  
204 resulting in a moderate torsion of the canal. The slender segment between the  
205 connection with the vestibule and the posterolateral tip of the lateral canal is straight,  
206 as in *Rudapithecus* (Fig. 1a-c), *Hoolock* (Fig. 1g) and most hominids (Fig. 1j-m), and  
207 laterally oriented, as in *Pongo* (Fig. 1j), some humans (Fig. 1m) and RUD 77 (Fig.  
208 1a-b). The ampullary portion of the lateral canal is bent superiorly, as in  
209 *Rudapithecus* (Fig. 1a-c) and extant hominoids (Fig. 1g-m). However, unlike extant  
210 great apes (Fig. 1j-l) and *Rudapithecus* (Fig. 1a-c), the portion between the ampulla  
211 and the tip of the lateral canal is inflated. The posterior canal is small and rounded,  
212 with a large ampulla. The CC is longer than in *Rudapithecus* (Fig. 1a-c) and in most  
213 extant great apes (with *Pongo* showing the shortest), yet more inflated (even if much  
214 less so than in orangutans; Fig. 1j), and the CC apex forms an obtuse angle. As in  
215 *Rudapithecus* and extant hominids, the planes identified by the lateral and posterior  
216 canals form a right angle and their trajectories do not intersect.

217

218 **Volumetric proportions.** Allometric regressions of SC volume vs. length were  
219 performed separately for hominoids and the rest of anthropoids included in the  
220 sample (Fig. 2a; measurements for the dryopiths are given in Supplementary Table  
221 1) because it has been previously shown that the former display an allometric grade  
222 shift toward relatively higher volumes at a comparable length once size-scaling

223 effects have been taken into account (5), with only minimal overlap. *Hispanopithecus*  
224 falls above the hominid regression line, while *Rudapithecus* is situated more (RUD  
225 77) or less (RUD 200) below the line, close to *Nacholapithecus*, but in all cases  
226 within the range of extant hominids and well above the regression line of other  
227 anthropoids (Fig. 2a). Gorillas are variable in this regard, while humans and  
228 orangutans display stouter proportions than chimpanzees and bonobos (Fig. 2b).  
229 The SCs of *Hispanopithecus* appear intermediate between these aforementioned  
230 taxa (closer to humans and orangutans), while those of *Rudapithecus*, *Oreopithecus*,  
231 and *Nacholapithecus* are slenderer and more comparable to those of chimpanzees  
232 and bonobos. Overall, given their range of variation, all the extinct apes analyzed  
233 here display extant hominid-like volumetric proportions of the vestibular apparatus.

234

235 **Shape analysis.** The bgPCA (Fig. 3), based on the deformation fields computed for  
236 the hominoid sample, allows us to discriminate extant hominoid species, as shown  
237 by classification results (99% of correctly classified individuals before and after cross  
238 validation). These results closely resemble those computed using a cross-validated  
239 bgPCA (Supplementary Fig.1). We also recover very significant group mean  
240 differences ( $p < 0.001$ ) for the raw shape data (Supplementary Table 2), confirming  
241 that group structure does not artifactually result from the bgPCA (52). Indeed, group  
242 differences account for a substantial amount of variance ( $R^2$ ) in the raw shape data,  
243 indicating that group separation is not spurious (52), although intergroup variance is  
244 increased to a similar extent by the standard bgPCA space and the cross-validated  
245 bgPCA (Supplementary Table 2).

246 bgPC1 (40.7% of the total variance) pulls apart hominids (mostly positive values)  
247 from hylobatids (negative values), with no overlap. Positive values along this axis

248 indicate short and bulgy SCs, together with a right angle between the anterior and  
249 posterior semicircular canals. Orangutans and humans display the most extreme  
250 condition due to the stoutness of their SCs. Chimpanzees, bonobos, and gorillas  
251 show a broad range of variation, with some individuals close to the origin due to their  
252 somewhat slenderer SCs (albeit less so than in hylobatids, which display negative  
253 values), and others overlapping with *Pongo* and *Homo*. Along bgPC1,  
254 *Hispanopithecus* overlaps with australopiths, extant great apes, and humans, while  
255 the *Rudapithecus* specimens fall within the African great ape range. Both RUD 77  
256 and RUD 200 closely approach the origin, with the latter showing slightly more  
257 positive values. *Oreopithecus* and *Nacholapithecus* are found on moderate negative  
258 values, within the lower range of *Pan* and *Gorilla*, due to their quite slender SCs  
259 (albeit clearly stouter than in hylobatids).

260 The patterns of shape variation captured by bgPC2 (33.4% of total variance; Fig.  
261 3a) reflect changes in the shape of three canals as well as their relative proportions.  
262 In particular, bgPC2 clearly discriminates *Homo* (with most negative values) from the  
263 rest of the sample, due to the presence in the former of a large and rounded  
264 (sometimes even slightly superiorly elongated) anterior canal, a posterolaterally  
265 displaced inferior portion of the posterior canal, and a small, fairly anterolaterally  
266 elongated lateral canal, whose slender portion connects to the vestibule more  
267 superiorly and anterolaterally than in apes. The latter fall on intermediate and  
268 positive values, with hylobatids considerably overlapping with *Pan* spp. (Fig. 3a). To  
269 a large extent, this is due to their anterior canal shape, which appears intermediate  
270 between the rounded morphology of humans and the marked vertical compression of  
271 *Pongo* and *Gorilla* (the latter taxa occupying more positive values with only very  
272 slight overlap with *Pan* and hylobatids). Both *Rudapithecus* and *Hispanopithecus*,

273 like *Oreopithecus* and *Nacholapithecus*, show intermediate values along this axis,  
274 overlapping with hylobatids and *Pan* spp. (as well as the *Australopithecus* specimen  
275 StW 573), but not with *Pongo* and *Gorilla*. Conversely, the other australopith (StW  
276 578) more closely approaches humans due to its larger vertical SCs.

277 bgPC3 (11.4% of variance; Fig. 3b) is driven by the shape of the anterior canal, its  
278 relative size relative compared with that of the lateral one, the length of the CC, and  
279 the amount of torsion of the lateral canal. Thus, negative values reflect a large and  
280 anterosuperiorly projecting anterior canal, coupled with a small lateral one, and a  
281 short CC. This axis discriminates *Pongo* (most negative values) from the rest of the  
282 sample, only minimally overlapping with some *Hylobates*. One individual of  
283 *Rudapithecus* (RUD 77) and *Oreopithecus* overlap with the range of orangutans due  
284 to their anterosuperiorly projecting anterior canal (albeit less so in RUD 77), short  
285 CC, and markedly small lateral canal. A similar morphology of the anterior canal is  
286 also found in some *Hylobates* and in one of the *Australopithecus* specimens (StW  
287 573), resulting in moderately negative scores. *Hispanopithecus* and the other  
288 individual of *Rudapithecus* (RUD 200) fall at the negative end of the gorilla and  
289 human variation, due to their intermediate anterior canal morphology, longer CC (yet  
290 less so than in most *Pan* and *Gorilla* individuals), and a larger lateral canal.  
291 *Nacholapithecus* and the other australopith specimen (StW 578) fall among  
292 moderate positive values, overlapping with gorillas, chimpanzees, bonobos, humans,  
293 and hylobatids, due to their long CC and more vertically aligned (i.e., superiorly  
294 directed) connection of the anterior canal with the CC.

295 When the inspected bgPCs are considered simultaneously to compute posterior  
296 probabilities of group membership (Table 1), the *Rudapithecus* RUD 77 individual  
297 occupies a position in the morphospace that does not fit well with most extant

298 hominoid genera ( $p < 0.05$ ), rather approaching the position of *Nacholapithecus* and  
299 *Oreopithecus* in the morphospace (Table 2). Conversely, RUD 200 shows  
300 considerable similarities with *Pan* ( $p = 0.549$ ) and *Nacholapithecus*. The three  
301 *Rudapithecus* specimens fall closer to one another than either approaches the single  
302 specimen of *Hispanopithecus* (Table 2), which is also more distant than  
303 *Nacholapithecus* from all the considered specimens (Table 2). *Hispanopithecus*  
304 mostly differs along bgPC1, sharing similarities in the volumetric proportions of the  
305 SCs and in the vertically compressed anterior canal morphology with  
306 *Australopithecus* individual StW 573 (Table 2). IPS18000 marginally differs from *Pan*  
307 ( $p = 0.053$ ) and is clearly an outlier compared to the remaining extant genera.

308 The cluster analyses based on the significant bgPCs (Fig. 4a) and raw shape data  
309 (Fig. 4b) further support the aforementioned results, since *Rudapithecus* and  
310 *Hispanopithecus* do not cluster with one another and show affinities with different  
311 taxa. In particular, the cluster based on the bgPCA results (Fig. 4a) indicates that  
312 *Rudapithecus* is most similar to both *Pan* and *Nacholapithecus*, while  
313 *Hispanopithecus* approaches hominins. This is further supported by the raw shape  
314 data cluster (Fig. 4b), which mainly differs by recovering a great ape cluster.

315

316 **Phylomorphospace and reconstruction of ancestral morphologies.** The shape  
317 data, as captured by the bgPCA performed on the extant hominoid sample,  
318 approaches the Brownian motion (BM) model of evolution, as supported by the  
319 phylogenetic signal computed for the bgPCs ( $K_{\text{mult}}=0.864$ ,  $p=0.019$ ) and for the raw  
320 data (i.e., the deformation fields;  $K_{\text{mult}}=0.863$ ,  $p=0.017$ ). We used phylogenetically  
321 informed techniques on the shape data to visualize the direction and magnitude of  
322 vestibular shape change during hominoid evolution as well as to depict the internal

323 nodes of the phylogeny—i.e., the inferred vestibular morphology of the last common  
324 ancestors (LCAs) of major groups—as reconstructed by maximum likelihood. The  
325 results are very similar irrespective of the precise phylogenetic placement of  
326 dryopiths as stem hominines (Fig. 5; Supplementary Fig. 2b), stem hominids  
327 (Supplementary Fig. 3a, c; Supplementary Fig. 2a), or stem pongines  
328 (Supplementary Fig. 3b, d; Supplementary Fig. 2c). The crown hominoid LCA (Figs.  
329 5, 6a) is reconstructed as possessing evenly-sized and moderately inflated SCs, a  
330 moderately long and not inflated CC, a fairly vertically compressed, yet not  
331 anterosuperiorly projecting, anterior canal, an almost rounded posterior canal, an  
332 obtuse angle between the planes identified by the anterior and posterior canals  
333 (close to the right angle), and a right angle among the SCs merging at the CC apex  
334 (Fig. 6a). Irrespective of the phylogenetic assumptions for dryopiths, the  
335 reconstructed LCA for crown hominoids is closer to hominids (especially  
336 *Nacholapithecus*, *Rudapithecus* and, among extant taxa, *Pan*) than to hylobatids  
337 (Fig. 5), in terms of their intermediate volumetric proportions, contrasting with the  
338 markedly slenderer SCs of gibbons and siamangs. In turn, the LCAs of crown  
339 hominines and dryopiths (*Rudapithecus* + *Hispanopithecus*) closely resemble one  
340 another irrespective of the underlying phylogenetic assumptions for the fossil species  
341 (Fig. 5, Supplementary Fig. 3), being extant-hominid-like in volumetric proportions  
342 but otherwise showing a more plesiomorphic morphology in the evenly sized and  
343 fairly rounded SCs.

344 The inferred LCA of crown hominids, in particular, closely resembles that of crown  
345 hominoids, except for the stouter volumetric proportions, more derived toward the  
346 extant hominid condition (Figs. 5, 6b). It displays equally-sized SCs, an obtuse to  
347 right angle in the apex of a moderately long CC, and a slightly laterally elongated

348 posterior canal (Fig. 6b). Orangutans appear derived from the LCA by displaying  
349 more inflated SCs (especially the anterior one, Figs. 1j, 6b), further diverging in the  
350 opposite direction from African great apes and humans because its short and  
351 extremely stout CC, as well as its anterosuperiorly projecting anterior canal and  
352 marked torsion of the lateral canal (Fig. 5b). The LCA of hominines (Fig. 6c) appears  
353 somewhat more derived than the LCAs of hominoids and hominids for both  
354 volumetric proportions and SC shape. It displays moderately stout SCs and  
355 medium/large vestibular recesses, equally developed SCs (with a slightly smaller  
356 lateral one), a vertically compressed anterior canal (more so than in any other LCA),  
357 a slightly laterally projecting posterior canal, and a long CC with an obtuse angle in  
358 its apex (Fig. 6c). *Homo* and *Gorilla* would have evolved in opposite directions from  
359 this ancestral morphology in terms of SC relative size, with humans showing the  
360 largest vertical canals (Figs. 1m, 5a) and gorillas displaying a larger lateral canal  
361 (Figs. 1k, 5a). Chimpanzees and bonobos, due to their equally sized SCs and fairly  
362 elongated CC (Figs. 1l, 5a), are closer to the hominine LCA morphology, while  
363 *Australopithecus* appears derived toward the human condition, due to the moderate  
364 increase in the size of the anterior and posterior canals (Fig 5). The reconstructed  
365 morphotype for the LCA of the investigated dryopiths (Fig. 6d) closely resembles  
366 those of hominines and hominids by displaying moderately stout and evenly-sized  
367 SCs (with a slightly smaller lateral one), an obtuse angle at the CC apex, and a not  
368 anterosuperiorly projecting anterior canal, differing from the hominid LCA by the  
369 somewhat less vertically compressed anterior canal (Fig. 6b,d).

370 *Hispanopithecus* and *Rudapithecus* appear to have diverged in opposite  
371 directions from their LCA (Fig. 5). The former seems derived in the volumetric  
372 proportions (similarly to, *Pongo*, *Australopithecus*, and *Homo*), whereas the



373 *Rudapithecus* condition in this regard is very similar to that of *Pan* as well as the  
374 reconstructed hominid LCA, and (to a lesser extent) to those of *Nacholapithecus* and  
375 *Oreopithecus* (Figs. 5, 6b). Likewise, the fairly short CC and a somewhat  
376 anterosuperiorly projecting anterior canal found in *Rudapithecus* (less so than in  
377 orangutans and *Oreopithecus*) contrast with the longer CC and the rectangular-  
378 shaped anterior canal found in *Hispanopithecus* (Fig. 1d). In these regards,  
379 *Hispanopithecus* more closely resembles the members of the African ape and  
380 human clade (Fig. 1a-c).

381 In summary, each extant hominid genus is derived in a particular direction from  
382 the ancestral morphology, with *Pan* remaining close to the hominid and hominine  
383 LCAs; *Nacholapithecus* appears as the least derived among both extant and fossil  
384 hominid taxa, together with *Oreopithecus*. The latter taxon also shows similarities  
385 with *Pongo* in the anterosuperiorly projecting anterior canal (Fig. 1e,j), despite being  
386 much slenderer in *Oreopithecus*. Overall, the dryopiths appear less derived than  
387 most extant genera relative to either the crown hominid or the crown hominine LCA,  
388 irrespective of their preferred phylogenetic placement. *Rudapithecus* appears more  
389 primitive than *Hispanopithecus*, being closer than the latter to both *Nacholapithecus*  
390 and *Oreopithecus*, and closely approaching both the reconstructed crown hominid  
391 LCA and *Pan* (Figs. 1, 5, 6). In contrast, *Hispanopithecus* is in some respects more  
392 derived than *Rudapithecus*, particularly toward orangutans, australopiths, and  
393 humans in the large vestibular recesses and in the stout SC volumetric proportions,  
394 and toward orangutans alone in the rounded posterior canal morphology (Fig. 5).  
395 Despite *Hispanopithecus* sharing its CC apex morphology (intermediate between  
396 African great apes and orangutans) and anterior canal shape (not anterosuperiorly  
397 projecting, yet not as squared as in gorillas) with *Homo* and *Australopithecus*, this

398 condition could be possibly plesiomorphic for hominids as a whole, as it is also found  
399 in the stem hominid *Nacholapithecus* (Fig 5). Overall, the two dryopiths share with  
400 African great apes and humans some features (moderately stout SCs, not  
401 anterosuperiorly projecting anterior canal, fairly long CC), but according to our  
402 analyses these features appear primitive (being likely present in the hominid LCA  
403 and, to a lesser extent, *Nacholapithecus*), with hominines (particularly gorillas) and  
404 especially orangutans having subsequently derived in opposite directions.

405

## 406 **Discussion**

407 Our results show that the vestibular morphology of both *Hispanopithecus* and  
408 *Rudapithecus* more closely resembles that of extant great apes and humans than  
409 that of hylobatids, in agreement with the current consensus that they belong to the  
410 great-ape-and-human clade (2-3, 6, 26). These similarities particularly concern the  
411 volumetric proportions of the SCs as well as the size of the latter relative to the  
412 vestibular recesses. Volumetric proportions, as reflected by the ratio between the  
413 volume and the length of the SCs, appear particularly relevant given that an  
414 allometric grade shift has been previously identified to characterize all extant  
415 hominids, so that they display relatively more voluminous SCs than other  
416 anthropoids (including hylobatids) at comparable lengths (5). The derived condition  
417 of hominids has been linked with locomotion (5), but is noteworthy that chimpanzees,  
418 bonobos, and gorillas are slightly more variable in SC volumetric proportions than  
419 orangutans and humans. Given the relationship between SC shape variation and  
420 locomotion noted by some authors (53-54), our results might reflect stronger  
421 locomotor-related selection pressures in orangutans and humans.

422 The classification results based on the bgPCA as well as the cluster analyses  
423 indicate that the two investigated dryopiths are distinguishable from one another,  
424 with the three specimens (two individuals) of *Rudapithecus* being more similar to one  
425 another than to the single specimen of *Hispanopithecus*. This result, together with  
426 other cranial differences (e.g., morphology of the frontal squama, premaxilla, and  
427 zygomatic), supports the distinction of these taxa at the genus rank (2-3, 7, 21, 25,  
428 35). *Rudapithecus* generally displays a somewhat more primitive morphology, closer  
429 to the one inferred for the crown hominid LCA. It shows some similarities with the  
430 fossil hominoids *Oreopithecus* and *Nacholapithecus*. The latter taxon appears more  
431 primitive than other hominids, in agreement with a previous study based on the  
432 entire inner ear morphology (49). However, both the hominid-like volumetric  
433 proportions of *Nacholapithecus* and the lack of a subarcuate fossa (55) support its  
434 stem hominid status, closely resembling the morphotype reconstructed for the crown  
435 hominid LCA. The morphology of *Rudapithecus* also resembles that of crown  
436 hominids such as *Pan* (volumetric proportions and the relative size of the SCs) and,  
437 to a lesser extent, orangutans (the somewhat anterosuperiorly projecting anterior  
438 canal and the short CC). As previously noted (5), chimpanzees and bonobos appear  
439 least derived than other extant hominids. This is shown by the possession of  
440 similarly-sized SCs (shared with the reconstructed crown hominid and crown  
441 hominine LCAs, while the dryopith LCA displays a slightly smaller lateral canal) and,  
442 especially, by the fairly slender volumetric proportions (intermediate between the  
443 hominine and hominid LCAs, yet closer to the latter). This is also supported by the  
444 similarities between *Pan* species and Miocene apes, especially *Nacholapithecus*.  
445 Nonetheless, chimpanzees and bonobos appear derived in some features (the small  
446 and rounded posterior canal as well as the obtuse angle of the CC apex), just like

447 gorillas and humans are derived in other directions (largest lateral canal relative to  
448 the other SCs and markedly enlarged vertical canals, respectively). Among  
449 hominids, orangutans and humans show the most extreme condition in the  
450 volumetric proportions of the SCs. Orangutans further diverge from the hominid LCA  
451 by the anterosuperiorly projecting anterior canal (even more so than in hylobatids).  
452 *Hispanopithecus* appears more derived than the other Miocene taxa, especially by  
453 the stouter SCs, while it does not fit well within the variation of any extant genus.  
454 More clearly than *Rudapithecus*, *Hispanopithecus* displays a mosaic of features that  
455 is unknown among extant hominids, including similarities with chimpanzees and  
456 bonobos (in the long CC), humans (the obtuse angle of the CC apex and the right  
457 angle between the planes of the posterior and lateral canals), and orangutans (the  
458 stout CC and the voluminous vestibular recesses, the latter also shared with  
459 humans) coupled with some unique features (the swollen area between the ampulla  
460 and the tip of the lateral canal, and the markedly inflated ampullae).

461 Interpreting the similarities of the investigated dryopiths in evolutionary terms is  
462 not straightforward. The results of the phylomorphospace approach and the  
463 reconstructed ancestral vestibular morphologies suggest that modern hominid-like  
464 volumetric proportions of the SCs would have been present in the LCA of crown  
465 hominids, while that of crown hominoids as a whole would have displayed somewhat  
466 intermediate proportions between hylobatids and hominids (yet closer to the latter).  
467 Differences in volumetric proportions of the SCs have been related to locomotor  
468 adaptations, because they directly affect the sensitivity and steadiness of the SCs in  
469 response to angular accelerations (5, 56). Hence, the moderately stout SCs of the  
470 LCA of crown hominids indicate that it showed a slow type of locomotion, which was  
471 present, to a large extent, also in the LCA of crown hominoids, as previously inferred

472 based on the size of the SC radius alone (41). Both *Rudapithecus* and  
473 *Hispanopithecus* show a wide gap between the lateral and posterior canals (the  
474 planes defined by them are well separated and do not intersect), caused by the  
475 anterolateral location of the lateral canal. This trait has been linked to orthograde  
476 behaviors (42), in agreement with the fossil evidence available for these taxa (6, 11,  
477 23, 25, 35, 57-61). However, from a phylogenetic viewpoint, the presence of the  
478 aforementioned feature in the investigated dryopiths is less informative than their  
479 hominid-like volumetric proportions, since the former have been identified as a  
480 synapomorphy of crown hominoids as a whole (5).

481 We conclude that, with differences that are consistent with their distinction at the  
482 genus rank, both *Hispanopithecus* and *Rudapithecus* display a unique hominid-like  
483 vestibular morphology that differs from that of any extant hominid genera but that  
484 appears quite close to that ancestral for crown hominids and crown hominines—  
485 mainly diverging from that of hylobatids by the stouter volumetric proportions of the  
486 SCs that are uniquely characteristic of great apes and humans among anthropoids.  
487 Orangutans appear most derived from such an ancestral vestibular morphology,  
488 whereas the investigated dryopiths lack most orangutan-like derived features—  
489 except for the slightly anterosuperiorly projecting anterior canal in *Rudapithecus*  
490 (also found in *Hylobates*) and some torsion in the shape of the lateral canal (a  
491 character that appears to be quite variable within hominoids). The lack of orangutan  
492 derived features in dryopithecines does not completely rule out a stem pongine  
493 status, as previously supported by some authors (10, 29-30), as it represents a more  
494 primitive morphology that probably precedes the subsequent evolution of the  
495 orangutan-like features in the pongine lineage. However, our results are more  
496 consistent with a stem hominid (6, 28) or a stem hominine (2-3, 14, 16, 25) status for

497 the investigated dryopiths. Our results suggest that African apes and hominin genera  
498 evolved in different directions from an ancestral morphology that more closely  
499 resembles that of *Pan* among extant hominines, and which is largely plesiomorphic  
500 for hominids, as further supported by similarities with the stem hominid  
501 *Nacholapithecus* (except for the slenderer volumetric proportions of the latter).  
502 Therefore, similarities between the SC morphology of the studied dryopiths and that  
503 of African apes do not necessarily imply a hominine status, but overall support the  
504 previous claim (5), based on extant taxa alone, that extant hominines evolved from  
505 an ancestral condition quite similar to that of the crown hominid LCA, and that the  
506 latter was characterized by derived volumetric proportions of the SCs. Pending the  
507 analysis of other Miocene apes, *Pan* among the extant taxa, and *Rudapithecus*  
508 among extinct apes, constitute the best available proxies for such ancestral  
509 morphologies, being already somewhat more derived from the crown hominoid  
510 condition that is best approximated by *Nacholapithecus*. In the future, the inclusion in  
511 the analyses of additional extinct hominoids will hopefully clarify further the  
512 evolutionary history of this hominoids during the Miocene.

513

## 514 **Materials and Methods**

515 **Sample Composition and Acquisition.** We inspected three petrosals from two  
516 individuals of *R. hungaricus* from Rudabánya, Hungary (RUD 77, left [RUD 77L] and  
517 right [RUD 77R]; and RUD 200, right) (12-13) and the single available petrosal of *H.*  
518 *laietanus* from Can Llobateres 2, Spain (IPS18000, right) (10, 29-30). The  
519 specimens of *Rudapithecus* are housed at the Geological Museum of the Mining and  
520 Geological Survey of Hungary (Hungary) and were scanned with a Skyscan 1172  
521 (obtaining a resolution of 0.0136 mm) at the Max Plank Institute for Evolutionary

522 Anthropology (Leipzig, Germany), with the following parameters: 100 kV voltage and  
523 100 mA. In turn, IPS18000 is housed at the Institut Català de Paleontologia Miquel  
524 Crusafont in Sabadell (Spain) and was scanned with a GE Phoenix V|Tome|X s 240  
525 (obtaining a resolution of 0.0295 mm) at the Centro Nacional de Investigación sobre  
526 la Evolución Humana (Burgos, Spain), with the following parameters: 125 kV voltage  
527 and 120 mA. The 3D virtual models of IPS18000, RUD 200 and RUD 77R were  
528 mirrored to enable the comparison with extant species. The segmented surfaces of  
529 the SCs of these fossils are available from MorphoSource  
530 (<https://www.morphosource.org>; see Supplementary Table 3).

531 The comparative sample for the volumetric proportion evaluation has been taken  
532 from a previous analysis that evaluated the phylogenetic signal embedded in the  
533 vestibule morphology (5), and integrated with recently published material of extant  
534 hominoids (4) and humans (62), together with the stem hominid *Nacholapithecus*  
535 *kerioi* (49). Overall, it consists of  $\mu$ CT scans of 169 dried crania and petrosals  
536 belonging to 27 extant anthropoid species, including all hominid genera and a  
537 selection of hylobatids, cercopithecoids, and platyrrhines, together with fossil taxa  
538 (Supplementary Table 3). The 3D meshes of the inner ear bony labyrinth of StW 573  
539 and StW 578 were downloaded from the Sterkfontein project of the digital repository  
540 MorphoSource.org. The juvenile status of a few specimens should not affect their  
541 vestibular morphology since the bony labyrinth ossifies in early prenatal stages and  
542 does not change subsequently (63). The analysis of the patterns of shape variation  
543 was focused on hominoids alone and was based on a subsample of 77 individuals  
544 representing all extant hominoid genera (Supplementary Table 4).

545 The  $\mu$ CT scans (voxel size for the extant and fossil specimens added in the  
546 present analysis to those originally published in ref. 5 can be found in in

547 Supplementary Table 5) were segmented using Avizo 9.0.1 (FEI Visualization  
548 Sciences Group) to digitally extract the left bony labyrinth, when available, or that  
549 from the right side (mirrored before the surface alignment). The vestibular apparatus  
550 was separated from the cochlea by cutting the generated 3D surfaces right under the  
551 saccule and the oval window and filling the resulting holes with Geomagic Studio  
552 2014 (3D Systems) using a flat surface (5).

553 The anatomical axes used for describing semicircular canal morphology  
554 corresponds to those employed in the vast majority of inner ear analysis focusing on  
555 primates (36-37,42,49), which conventionally follow the same orientation as in  
556 humans (i.e., superior/inferior and anterior/posterior).

557 **Shape Analysis.** Shape was analyzed using a deformation-based 3DGM  
558 technique that does not rely on a priori defined landmarks and examines the  
559 geometrical correspondences between continuous surfaces (5, 48, 64-66). This  
560 method quantifies the deformation from the analyzed surfaces from a constructed  
561 sample-average surface (template) (64, 66), mathematically models them as a  
562 diffeomorphism, and computes a set of vectors (momenta) that describe the direction  
563 and magnitude of deformation from the average template. The unscaled 3D models  
564 were aligned with Avizo 9.0.1 using the 'Align Surface' module before running the  
565 analyses. The diffeomorphisms and the momenta were computed in the Barcelona  
566 Supercomputing Center (BSC) (Barcelona, Spain) with Deformetrica 4 software. The  
567 3D models of the fossils were projected a posteriori in the tangent space generated  
568 by means of between-group principal components analysis (bgPCA) ran on the set  
569 of momenta for the hominoid-only sample using genera as grouping factor. The  
570 bgPCA was computed in R Studio v.1.1.453 for R v.3.5.0 using the *ade4* package  
571 (67), while the cross-validated bgPCA was derived using the 'groupPCA' function of



572 the *Morpho* v2.6 (68) library. Group mean differences were tested by computing a  
573 permutational ANOVA (1000 permutations) based on the Euclidean distance  
574 between the means using the 'adonis' function of the *Vegan* package (69). The  
575 amount of variance ( $R^2$ ) explained by group differences in the raw shape data, and in  
576 the scores of both standard and cross-validated bgPCA results, was estimated with  
577 the same function as for the permutation test. To further assess similarities between  
578 the analyzed fossil taxa and extant hominoid genera in terms of vestibular  
579 morphology, we computed Mahalanobis squared distances ( $D^2$ ) between the bgPC  
580 scores of fossils and group centroids used in the bgPCA. The distances were also  
581 used to compute the posterior probabilities of group membership for the fossil  
582 specimens by means of the 'typprobClass' function of the *Morpho* v2.6 (68) package,  
583 on the basis of the multivariate normal distribution of extant groups defined a priori in  
584 the bgPCA analyses. The similarities between extant and fossil hominoids were  
585 further investigated by means of a cluster analysis (UPGMA) on the aforementioned  
586  $D^2$  and on the Euclidean distances between pairs of species mean configurations for  
587 the raw data using the 'average' method of the 'hclust' function of the 'stats' package  
588 in R

589 Additionally, the correlation between the log-transformed cube root of SC volume  
590 ( $\ln \text{VolSC}$ , in mm) and log-transformed SC length ( $\ln L$ , in mm) was assessed means  
591 of ordinary least-squares (OLS) linear regression, as the relationship between these  
592 variables has previously been shown to display an allometric grade shift between  
593 hominids and other anthropoids (5). Two separate regressions were computed for  
594 the non-hominid anthropoids and for great apes and humans using SPSS Statistics  
595 v. 17.0 for Windows (see Fig. 7b in ref. 5). The regression for the non-hominid  
596 sample was used as a baseline for computing the allometric residuals

597 (Supplementary Table 1; see Table 5 in ref. 5) for the extant and extinct species.  
598 Comparisons between the latter and extant groups are depicted by means of box-  
599 and-whisker plots.

600

601 **Phylomorphospace and phylogenetic signal.** Major patterns of vestibular shape  
602 variation were quantified using a phylomorphospace approach (70), obtained by  
603 projecting a phylogeny on to the tangent space derived from the bgPCA of a 3DGM  
604 shape analysis. In this method, the tips of the phylogeny correspond to the genus  
605 bgPC centroid, while the internal nodes (i.e., the ancestral states) of the tree are  
606 estimated using a maximum likelihood method for continuous characters, assuming  
607 that the reconstructed nodes approximate the true morphology of the ancestors.  
608 Thus, when a time-calibrated phylogeny is used, its two-dimensional representation  
609 enables the intuitive interpretation of the magnitude and direction of evolution, based  
610 on branch length and orientation. The molecular-based phylogenetic tree for extant  
611 hominoids used in this analysis was downloaded from the 10kTrees Website (ver. 3;  
612 <http://10ktrees.fas.harvard.edu/>), while *Hispanopithecus* and *Rudapithecus* were  
613 added based on the assumption that they are closely related and constitute a clade,  
614 with the tips corresponding to 9.6 Ma and 10.1 Ma, respectively (20), and diverging  
615 at 11.1 Ma, but considering three different phylogenetic placements for these taxa as  
616 discussed in the literature during the last two decades (see above): stem hominids,  
617 stem hominines, and stem pongines (Supplementary Fig. 2). Analyses were  
618 repeated based on the resulting three different cladograms and their results  
619 compared to evaluate the effect of phylogenetic uncertainties surrounding these  
620 taxa. *Oreopithecus* is here considered as a stem hominoid as indicated by most  
621 recent cladistic analyses (4). *Nacholapithecus* has been included in a stem hominid

622 position, 2 Myr older than the divergence between pongines and hominines (crown  
623 hominids), thus always preceding the divergence of dryopiths in all the phylogenetic  
624 hypotheses, and its tip corresponds to 14.77 Ma (54, 71). The divergence between  
625 crown hominoids and *Oreopithecus* has been placed 1 Myr older than the  
626 divergence between hylobatids and hominids and its tip corresponds to its last  
627 occurrence in the fossil record (7.0-6.5 Ma; ref. 72). For the South African  
628 *Australopithecus* sp., we used the published first appearance datum for  
629 *Australopithecus africanus* (4.02 Ma) that includes the Jacovec specimens into the  
630 species (73).

631 The position in the morphospace of the internal nodes of the phylogeny (ancestral  
632 morphologies) was estimated via a maximum likelihood method for continuous  
633 characters (74) using the 'fastAnc' function of *phytools* v. 0.6-60 R package (75).  
634 Subsequently, the bgPC scores of the ancestral states were rotated and translated  
635 from the shape data back into the configuration space for interpolation and 3D  
636 visualization using Deformetrica 3 software.

637 The phylogenetic signal embedded in vestibular shape, as captured by all the  
638 bgPCs, was quantified by means of the multivariate phylogenetic index  $K_{\text{mult}}$  (76)  
639 using *geomorph* v3.1.1 (77) R package. The  $K_{\text{mult}}$  statistic, like its univariate  
640 counterpart (77), assesses the amount of phylogenetic signal relative to that  
641 expected for character undergoing Brownian motion and reflects the accuracy with  
642 which the phylogenetic tree describes the variance-covariance pattern found in the  
643 shape data. It is also informative about the accumulation of the variance in the  
644 phylogeny. Thus,  $K_{\text{mult}} \approx 1$  is obtained when the inspected mode of evolution can  
645 adequately be described using a stochastic Brownian motion model. For  $K_{\text{mult}} < 1$ ,  
646 the majority of the variance is found within clades, thus implying that neighbor taxa

647 resemble one another less than expected and that the mode of evolution is not  
648 aleatory, possibly as the results of homoplastic adaptations (i.e., related to function  
649 rather than phylogeny). Values of  $K_{\text{mult}} > 1$  indicate that variance is mostly found  
650 among different clades, being obtained when close taxa are less diverse than  
651 expected under Brownian motion (suggesting that phenomena of stabilizing selection  
652 might have occurred).

653

### 654 **Acknowledgements**

655 This research has been funded by the Agencia Estatal de Investigación (CGL2016-  
656 76431-P and CGL2017-82654-P, AEI/FEDER EU; and BES-2015-071318 to A.U.),  
657 the Generalitat de Catalunya (CERC A Programme), the consolidated research  
658 groups 2017 SGR 86 and 2017 SGR 116 GRC, and the French Centre National de  
659 la Recherche Scientifique. Part of the analyses were performed using Barcelona  
660 Supercomputing Center resources (BCV-2020-1-0008). We thank Jose Braga for  
661 allowing us to use the CT scans of the human specimens; the Max Plank Institute for  
662 providing access to the microCT scans of RUD 77 and RUD 200; the ESRF heritage  
663 database for palaeontology, evolutionary biology and archaeology, for providing  
664 access to a part of the hominoid scans used in the present analysis; and Lynn  
665 Copes, Lynn Lucas, and the Museum of Comparative Zoology (Cambridge, MA) for  
666 providing access to a part of the scans used in the study, originally appearing in refs.  
667 79 and 80, and funded by NSF DDIG #0925793, and a Wenner-Gren Foundation  
668 Dissertation Grant #8102 (both to Lynn Copes). These scans were downloaded from  
669 MorphoSource.org, a web-accessible archive for 3D digital data housed by Duke  
670 University. A.B. was funded by the University of the Witwatersrand.

671

672 **References**

- 673 1. N. J. Stevens, et al., Palaeontological evidence for an Oligocene divergence  
674 between Old World monkeys and apes. *Nature* **497**, 611–614 (2013).
- 675 2. D. R. Begun, “The Miocene hominoid radiation“ in A companion to  
676 Paleoanthropology D. R. Begun, Ed. (Blackwell Publishing, 2013), pp. 398–  
677 416.
- 678 3. D. R. Begun, “Fossil record of Miocene hominoids” in Handbook of  
679 Paleoanthropology, 2nd edn, W. Henke, I. Tattersall, Eds. (Springer, 2015),  
680 pp. 1261–1332.
- 681 4. I. Nengo, et al., New infant cranium from the African Miocene sheds light on  
682 ape evolution. *Nature* **548**, 169–174 (2017).
- 683 5. A. Urciuoli, C. Zanolli, J. Dumoncel, S. Moyà-Solà, D. M. Alba, The evolution  
684 of the vestibular apparatus in apes and humans. *eLife* **9** (2020)
- 685 6. D. M. Alba, Fossil apes from the Vallès-Penedès Basin. *Evol. Anthropol.* **21**,  
686 254–269 (2012).
- 687 7. Begun, D. R. Miocene hominids and the origins of the African apes and  
688 humans. *Ann. Rev. Anthropol.* **39**, 67–84 (2010).
- 689 8. J. Kelley, “The hominoid radiation in Asia” in The Primate Fossil Record, W.  
690 C. Hartwig, Ed. (Cambridge University Press, 2002), pp. 369–384.
- 691 9. P. Andrews, T. Harrison, E. Delson, R. L. Bernor, L. Martin, “Distribution and  
692 biochronology of European and Southwest Asian Miocene catarrhines” in The  
693 Evolution of Western Eurasian Neogene Mammal Faunas, R. L. Bernor, V.  
694 Fahlbusch & H.-W. Mittmann, Eds. (Columbia University Press, 1996), pp.  
695 168–207.

- 696 10. S. Moyà-Solà, M. Köhler, Recent discoveries of *Dryopithecus* shed new light  
697 on evolution of great apes. *Nature* **365**, 543 (1993).
- 698 11. S. Moyà-Solà, M. Köhler, A *Dryopithecus* skeleton and the origins of great-  
699 ape locomotion. *Nature* **379**, 156–159 (1996).
- 700 12. L. Kordos, Begun, R. D., A new reconstruction of RUD 77, a partial cranium of  
701 *Dryopithecus brancoi* from Rudabánya, Hungary. *Am. J. Phys. Anthropol.*  
702 **103**, 277–294 (1997).
- 703 13. L. Kordos, D. R. Begun, A new cranium of *Dryopithecus* from Rudabánya,  
704 Hungary. *J. Hum. Evol.* **41**, 689–700 (2001).
- 705 14. D. R. Begun, C. V. Ward, M. D. Rose, “Events in hominoid evolution” in  
706 Function, Phylogeny and Fossils: Miocene Hominoid Evolution and  
707 Adaptation, D. R. Begun, C. V. Ward, M. D. Rose (Plenum Press, 1997), pp.  
708 389–415.
- 709 15. D. R. Begun, “African and Eurasian Miocene hominoids and the origins of the  
710 Hominidae” in Hominoid Evolution and Environmental Change in the Neogene  
711 of Europe, Vol 2. Phylogeny of the Neogene Hominoid Primates of Eurasia, L.  
712 D. Bonis, G. Koufos, P. Andrews, Eds. (Cambridge University Press, 2001),  
713 pp. 231–253.
- 714 16. D. R. Begun, “The pliopithecoidea” in: The Primate Fossil Record, W. Hartwig,  
715 Ed. (Cambridge University Press., 2002), pp. 339–368.
- 716 17. S. Moyà-Solà, M. Köhler, D. M. Alba, I. Casanovas-Vilar, J. Galindo,  
717 *Pierolapithecus catalaunicus*, a new Middle Miocene great ape from Spain.  
718 *Science* **306**, 1339–1344 (2004).
- 719 18. S. Moyà-Solà, et al., First partial face and upper dentition of the Middle  
720 Miocene hominoid *Dryopithecus fontani* from Abocador de Can Mata (Vallès-

- 721 Penedès Basin, Catalonia, NE Spain): taxonomic and phylogenetic  
722 implications. *Am. J. Phys. Anthropol.* **139**, 126–145 (2009).
- 723 19. S. Moyà-Solà, et al., A unique Middle Miocene European hominoid and the  
724 origins of the great ape and human clade. *Proc. Natl. Acad. Sci. U.S.A.* **106**,  
725 9601–9606 (2009).
- 726 20. I. Casanovas-Vilar, et al., Updated chronology for the Miocene hominoid  
727 radiation in Western Eurasia. *Proc. Natl. Acad. Sci. U.S.A.* **108**, 5554–5559  
728 (2011).
- 729 21. D. R. Begun, Dryopithecins, Darwin, de Bonis, and the European origin of the  
730 African apes and human clade. *Geodiversitas* **31**, 789–816 (2009).
- 731 22. D. M. Alba, et al., New dental remains of *Hispanopithecus laietanus*  
732 (Primates: Hominidae) from Can Llobateres 1 and the taxonomy of Late  
733 Miocene hominoids from the Vallès-Penedès Basin (NE Iberian Peninsula). *J.*  
734 *Hum. Evol.* **63**, 231–246 (2012).
- 735 23. D. M. Alba, S. Almécija, I. Casanovas-Vilar, J. M. Méndez, S. Moyà-Solà, A  
736 partial skeleton of the fossil great ape *Hispanopithecus laietanus* from Can  
737 Feu and the mosaic evolution of crown-hominoid positional behaviors. *PLoS*  
738 *ONE* **6**, e39617 (2012).
- 739 24. D. R. Begun, *Sivapithecus* is east and *Dryopithecus* is west, and never the  
740 twain shall meet. *Anthropol. Sci.* **113**, 53–64 (2005).
- 741 25. D. R. Begun, M. C. Nargolwalla, L. Kordos, European Miocene hominids and  
742 the origin of the African ape and human clade. *Evol. Anthropol.* **21**, 10–23  
743 (2012).
- 744 26. P. Andrews, Last common ancestor of apes and humans: morphology and  
745 environment. *Folia Primatol.* **91**, 1–27 (2020).

- 746 27. M. Böhme, et al. A new Miocene ape and locomotion in the ancestor of great  
747 apes and humans. *Nature* **575**, 489–493 (2019).
- 748 28. D. M. Alba, et al., Miocene small-bodied ape from Eurasia sheds light on  
749 hominoid evolution. *Science* **350**, aab2625 (2015).
- 750 29. M. Köhler, S. Moyà-Solà, D. M. Alba, “Eurasian hominoid evolution in the light  
751 of recent *Dryopithecus* findings” in: Hominoid Evolution and Environmental  
752 Change in the Neogene of Europe, Vol 2. Phylogeny of the Neogene  
753 Hominoid Primates of Eurasia, L. D. Bonis, G. Koufos, P. Andrews, Eds.  
754 (Cambridge University Press, 2001), pp. 192–212.
- 755 30. S. Moyà-Solà, M. Köhler, New partial cranium of *Dryopithecus* Lartet, 1863  
756 (Hominoidea, Primates) from the upper Miocene of Can Llobateres,  
757 Barcelona, Spain. *J. Hum. Evol.* 29, 101–139 (1995).
- 758 31. D. R. Begun, L. Kordos, “Phyletic affinities and functional convergence in  
759 *Dryopithecus* and other Miocene and living hominids.” in Function, Phylogeny,  
760 and Fossils: Miocene Hominoid Evolution and Adaptions, D.R., Begun, C.V.,  
761 Ward, M.D., Rose Eds. (Plenum Press, 1997), pp. 291–316.
- 762 32. D. R. Begun, How to identify (as opposed to define) a homoplasy: Examples  
763 from fossil and living great apes. *J. Hum. Evol.* **52**, 559–572 (2007).
- 764 33. S. G. Larson, Parallel evolution in the hominoid trunk and forelimb. *Evol.*  
765 *Anthropol.* **6**, 87–99 (1998).
- 766 34. T. C. Rae, Mosaic evolution in the origin of the Hominoidea. *Folia Primatol.*  
767 **70**, 125–135 (1999).
- 768 35. C. V. Ward, “Postcranial and locomotor adaptations of hominoids” in  
769 Handbook of Paleoanthropology, 2nd edn W. Henke, I. Tattersall, Eds.  
770 (Springer, 2015), pp. 1363–1386.



- 771 36. F. Spoor, B. Wood, F. Zonneveld, Implications of early hominid labyrinthine  
772 morphology for evolution of human bipedal locomotion. *Nature* **369**, 645–648  
773 (1994).
- 774 37. F. Spoor, F. Zonneveld, Comparative review of the human bony labyrinth.  
775 *Yearb. Phys. Anthropol.* **41**, 211–251 (1998).
- 776 38. Spoor, F. et al., The primate semicircular canal system and locomotion. *Proc.*  
777 *Natl. Acad. Sci U.S.A.* **104**, 10808–10812 (2007).
- 778 39. David, R., et al., Motion from the past. A new method to infer vestibular  
779 apparatus capacities of extinct species. *C. R. Palevol* **9**, 397–410 (2010).
- 780 40. David, R., A. Stoessel, A. Berthoz, F. Spoor, D. Bennequin, Assessing  
781 morphology and function of the semicircular duct system: introducing new in-  
782 situ visualization and software toolbox. *Sci. Rep.* **6**, 32772 (2016).
- 783 41. T. M. Ryan, et al., Evolution of locomotion in Anthropeidea: the semicircular  
784 canal evidence. *Proc. R. Soc. B* **279**, 3467–3475 (2012).
- 785 42. A. Le Maître, P. Schuetz, P. Vignaud, M. Brunet, New data about semicircular  
786 canal morphology and locomotion in modern hominoids. *J. Anat.* **231**, 95–109  
787 (2017).
- 788 43. L. Rook, et al., The bony labyrinth of *Oreopithecus bambolii*. *J. Hum. Evol.* **46**,  
789 347–354 (2004).
- 790 44. M. S. Ponce de León, et al., Human bony labyrinth is an indicator of  
791 population history and dispersal from Africa. *Proc. Natl. Acad. Sci. U.S.A.* **115**,  
792 4128–4133 (2018).
- 793 45. A. Beaudet, The inner ear of the *Paranthropus* specimen DNH 22 from  
794 Drimolen, South Africa. *Am. J. Phys. Anthropol.* **170**, 439–446 (2019).

- 795 46. A. Beaudet, et al., The bony labyrinth of StW 573 (“Little Foot”): Implications  
796 for early hominin evolution and paleobiology. *J. Hum. Evol.* **127**, 67–80  
797 (2019).
- 798 47. J. del Rio, et al., Allometry, function and shape diversification in the inner ear  
799 of platyrrhine primates. *J. Mammal. Evol.* (2020) DOI:  
800 <https://doi.org/10.1007/s10914-019-09490-9>
- 801 48. A. Urciuoli, C. Zanolli, S. Almécija, S. Moyà-Solà, D. M. Alba, Analysis of the  
802 primate vestibular apparatus: a comparison of landmark-based and  
803 deformation-based 3D geometric morphometric approaches. *Proc. Eur. Soc.*  
804 *Stud. Hum. Evol.* **7**, 193 (2018).
- 805 49. N. Morimoto, et al., Variation of bony labyrinthine morphology in  
806 Mio–Plio–Pleistocene and modern anthropoids. *Am. J. Phys. Anthropol.* **173**,  
807 276–293 (2020)
- 808 50. T. C. Rae, P. M. Johnson, W. Yano, E. Hirasaki, Semicircular canal size and  
809 locomotion in colobine monkeys: a cautionary tale. *Folia Primatol.* **87**, 213–  
810 223 (2016).
- 811 51. D. M. Malinzak, R. F. Kay, T. E. Hullar, Locomotor head movements and  
812 semicircular canal morphology in primates. *Proc. Natl. Acad. Sci. U.S.A.* **109**,  
813 17914–17919 (2012).
- 814 52. A. Cardini, P. D. Polly, Cross-validated between-group PCA scatterplots: A  
815 solution to spurious group separation? *Evol. Biol.* **47**, 85–95 (2020).
- 816 53. A. Perier, R. Lebrun, L. Marivaux, Different level of intraspecific variation of  
817 the bony labyrinth morphology in slow- versus fast-moving Primates. *J.*  
818 *Mammal. Evol.* **23**, 353–368 (2016).

- 819 54. L. A. Gonzales, M. D. Malinzak, R. F. Kay, Intraspecific variation in  
820 semicircular canal morphology—A missing element in adaptive scenarios?  
821 *Am. J. Phys. Anthropol.* **168**, 10–24 (2019).
- 822 55. Y. Kanimatsu, M. Nakatsukasa, D. Shimizu, Y. Nakano, H. Ishida, Loss of the  
823 subarcuate fossa and the phylogeny of *Nacholapithecus*. *J. Hum. Evol.* **131**,  
824 22–27 (2019).
- 825 56. R. D. Rabbitt, E. R. Damiano, J. W. Grant, “Biomechanics of the Semicircular  
826 Canals and Otolith Organs” in *The Vestibular System* S. M. Highstein, R. R.  
827 Fay, A. N. Popper, Eds. (Springer, 2004) pp. 153–201.
- 828 57. D. R. Begun, Phyletic diversity and locomotion in primitive European  
829 hominids. *Am. J. Phys. Anthropol.* **87**, 311–340 (1992).
- 830 58. D. R. Begun, New catarrhine phalanges from Rudabánya (Northeastern  
831 Hungary) and the problem of parallelism and convergence in hominoid  
832 postcranial morphology. *J. Hum. Evol.* **24**, 373–402 (1993).
- 833 59. S. Almécija, D. M. Alba, S. Moyà-Solà, M. Köhler, Orang-like manual  
834 adaptations in the fossil hominoid *Hispanopithecus laietanus*: first steps  
835 towards great ape suspensory behaviours. *Proc. R. Soc. B* **274**, 2375–2384  
836 (2007).
- 837 60. D. M. Alba, S. Almécija, S. Moyà-Solà, Locomotor inferences in  
838 *Pierolapithecus* and *Hispanopithecus*: reply to Deane and Begun (2008). *J.*  
839 *Hum. Evol.* **59**, 143–149 (2010).
- 840 61. M. Pina, D. M. Alba, S. Almécija, J. Fortuny, S. Moyà-Solà, Brief  
841 communication: paleobiological inferences on the locomotor repertoire of  
842 extinct hominoids based on femoral neck cortical thickness: the fossil great

- 843 ape *Hispanopithecus laietanus* as a test-case study. *Am. J. Phys. Anthropol.*  
844 **149**, 142–148 (2012).
- 845 62. W. Wimmer, C. Vandersteen, N. Guevara, M. Caversaccio, H. Delingette, H.,  
846 “Robust cochlear modiolar axis detection in CT” in *Medical Image Computing*  
847 *and Computer Assisted Intervention – MICCAI 2019* D. Shen, et al. Eds.  
848 (Springer, 2019), pp. 3–10.
- 849 63. N. Jeffery, F. Spoor, Prenatal growth and development of the modern human  
850 labyrinth. *J. Anat.* **204**, 71–92 (2004).
- 851 64. S. Durrleman, et al., “Topology preserving atlas construction from shape data  
852 without correspondence using sparse parameters” in *Proceedings of Medical*  
853 *Image Computing and Computer Aided Intervention* N. Ayache, H. Delingette,  
854 P. Golland, K. Mori (Springer, 2012), pp. 223–230.
- 855 65. J. Dumoncel, S. Durrleman, J. Braga, J. P. Jessel, G. Subsol, Landmark-free  
856 3D method for comparison of fossil hominins and hominids based on  
857 endocranium and EDJ shapes. *Am. J. Phys. Anthropol.* **153**, 114 (2014).
- 858 66. A. Beaudet, et al., Upper third molar internal structural organization and  
859 semicircular canal morphology in Plio-Pleistocene South African  
860 cercopithecoids. *J. Hum. Evol.* **95**, 104–120 (2016).
- 861 67. S. Dray, A. Dufour, The ade4 Package: Implementing the duality diagram for  
862 ecologists. *J. Stat. Softw.* **22**, (2007).
- 863 68. S. Schlager, “Morpho and Rvcg - Shape Analysis in R.” in: *Statistical Shape*  
864 *and Deformation Analysis*, G. Zheng, S. Li, G. Szekely Eds. (Academic  
865 Press., 2017) pp. 217–256.
- 866 69. J. Oksanen, et al., *vegan: Community Ecology Package*. R package version  
867 2.5-6. <https://CRAN.R-project.org/package=vegan>

- 868 70. B. Sidlauskas, Continuous and arrested morphological diversification in sister  
869 clades of characiform fishes: A phylomorphospace approach. *Evolution* **62**,  
870 3135–3156 (2008).
- 871 71. M. Nakatsukasa, Y. Kunimatsu, *Nacholapithecus* and its importance for  
872 understanding hominoid evolution. *Evol. Anthropol.* **18**, 103–119 (2009).
- 873 72. L. Rook, L. Bondioli, M. Köhler, S. Moyà-Solà, R. Macchiarelli, *Oreopithecus*  
874 was a bipedal ape after all: evidence from the iliac cancellous architecture.  
875 *Proc. Natl. Acad. Sci U.S.A.* **96**, 8795–8799 (1999).
- 876 73. B. Wood, E. K. Boyle, Hominin taxic diversity: Fact or fantasy? *Am. J. Phys.*  
877 *Anthropol.* **159**, 37–78 (2016).
- 878 74. D. Schluter, T. Price, A. Ø. Mooers, D. Ludwig, Likelihood of ancestor states  
879 in adaptive radiation. *Evolution* **51**, 1699–1711 (1997).
- 880 75. L. J. Revell, phytools: An R package for phylogenetic comparative biology  
881 (and other things). *Methods Ecol. Evol.* **3**, 217–223 (2012).
- 882 76. D. C. Adams, A generalized K statistic for estimating phylogenetic signal from  
883 shape and other high-dimensional multivariate data. *Syst. Biol.* **63**, 685–697  
884 (2014).
- 885 77. D. C. Adams, M. L. Collyer, A. Kaliontzopoulou, Geomorph: Software for  
886 geometric morphometric analyses. R package version 3.1.0. [https://cran.r-](https://cran.r-project.org/package=geomorph)  
887 [project.org/package=geomorph](https://cran.r-project.org/package=geomorph) (2019).
- 888 78. S. P. Blomberg, J. T. Garland, A. R. Ives, Testing for a phylogenetic signal in  
889 comparative data: behavioural traits are more labile. *Evolution* **57**, 717–745  
890 (2003).
- 891 79. L. E. Copes, W. H. Kimbel, Cranial vault thickness in primates: *Homo erectus*  
892 does not have uniquely thick vault bones. *J. Hum. Evol.* **90**, 120–134 (2016).

893 80. L. E. Copes, L. M. Lucas, J. O. Thostenson, H. E. Hoekstra, A collection of  
894 non-human primate computed tomography scans housed in MorphoSource, a  
895 repository for 3D data. *Sci. Data* **3**, 1 (2016).

896 **FIGURE CAPTIONS**

897 **Fig. 1.** The vestibular apparatus morphology of *Rudapithecus hungaricus* (**a-c**),  
898 *Hispanopithecus laietanus* (**d**), fossil hominoids (**e-f**), and individuals from extant  
899 hominoid genera (**g-m**) as depicted by renderings of the 3D models. From left to  
900 right, in posterolateral, superior, and posteromedial views: (**a**) *R. hungaricus* (RUD  
901 77L); (**b**) *R. hungaricus* (RUD 77R); (**c**) *R. hungaricus* (RUD 200); (**d**) *H. laietanus*  
902 (IPS18000); (**e**) *Oreopithecus bambolii* (BAC 208); (**f**) *Nacholapithecus kerioi* (BG  
903 42744); (**g**) *Hoolock hoolock* (AMNH.M 83425); (**h**) *Symphalangus syndactylus*  
904 (AMNH.M 106583); (**i**) *Hylobates lar* (MCZ 41424); (**j**) *Pongo* sp.(IPS10647); (**k**)  
905 *Gorilla gorilla* (AMNH.M 167338); (**l**) *Pan troglodytes* (AMNH.M 51204); (**m**) *Homo*  
906 *sapiens* (F 04). Scale bars = 5 mm

907

908 **Fig. 2.** (**a**) Allometric regressions of cube root of semicircular canal volume (In  
909 VolSC, in mm) vs. semicircular canal length (In L, in mm) in anthropoids. Lines  
910 represent ordinary least-squares (OLS) best-fit lines for extant hominids (red) and  
911 other extant anthropoids (blue). Both hominids and other anthropoids show a  
912 negatively allometric relationship between VolSC and L, but with a marked allometric  
913 grade shift—such that hominids possess stouter canals than other anthropoid taxa at  
914 comparable lengths (see Supplementary Table 1 for comparative sample  
915 measurements). (**b**) Boxplots of allometric residuals computed using the best-fit line  
916 of the non-hominid anthropoid regression as baseline. Horizontal line is the median,  
917 boxes represent the interquartile range, whiskers represent maximum and minimum  
918 excluding outliers (beyond 1.5 times the upper and lower quartiles), and black dots  
919 are outliers. Samples for each boxplot are: Platyrrhini ( $n=15$ ), Cercopithecoidea  
920 ( $n=80$ ), Hylobatidae ( $n=23$ ), *Gorilla* ( $n=8$ ), *Pongo* ( $n=8$ ), *Pan* ( $n=25$ ), and *Homo*

921 ( $n=10$ ). Note that all the fossils overlap with extant hominoids. However, while  
922 *Australopithecus* (StW 573 and StW 578) and *Hispanopithecus* (IPS18000)  
923 approach the human and orangutan condition, *Rudapithecus* RUD 200 and  
924 *Oreopithecus* (BAC 208) only overlap with African apes, while *Nacholapithecus* (BG  
925 42744) and *Rudapithecus* RUD 77 only overlap with chimpanzees and bonobos, and  
926 marginally also with the upper range of hylobatids and cercopithecoids.

927

928 **Fig. 3.** Results of the bgPCA based on vestibular shape (as reflected by deformation  
929 data) in hominoids using genera as grouping factor (variance explained by each  
930 bgPC is included within parentheses): (a) bgPC2 vs. bgPC1; (b) bgPC3 vs. bgPC1.  
931 Extreme conformations for each bgPC are displayed: (c) bgPC1; (d) bgPC2; (e)  
932 bgPC3. Convex hulls are drawn for each hominoid genus and colored as follows:  
933 blue, *Pongo*; black, *Gorilla*; green, *Pan*; lilac, *Homo*; red, *Hylobates*; orange,  
934 *Symphalangus*; cyan, *Hoolock*.

935

936 **Fig. 4.** Dendrograms resulting from UPGMA cluster analyses based on: (a) the  
937 Mahalanobis squared distances ( $D^2$ ) computed for the meaningful between-group  
938 principal components (bgPC1–bgPC3, 86% of variance) depicted in Figure 2  
939 (cophenetic correlation: 0.75); (b) the Euclidean distances computed for the raw  
940 shape data (i.e., the deformation fields) obtained from the deformation-based 3D  
941 geometric morphometrics analysis (cophenetic correlation: 0.77).

942

943 **Fig. 5.** Phylomorphospaces of the vestibular apparatus in hominoids, obtained by  
944 projecting the phylogenetic tree that considers dryopithecines a clade of stem  
945 hominines (Supplementary Fig. 1b) on bivariate plots between bgPCs. The tips

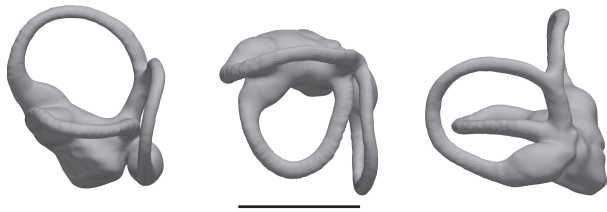


946 correspond to genus bgPCA score centroids: **(a)** bgPC2 vs. bgPC1; **(b)** bgPC3 vs.  
947 bgPC1. Key ancestral morphologies reconstructed using maximum likelihood for the  
948 last common ancestors (LCAs) of various clades are depicted by means of  
949 arrowheads. See Supplementary Fig. 2 for the results based on alternative  
950 phylogenetic hypotheses (Supplementary Fig. 1a,c).

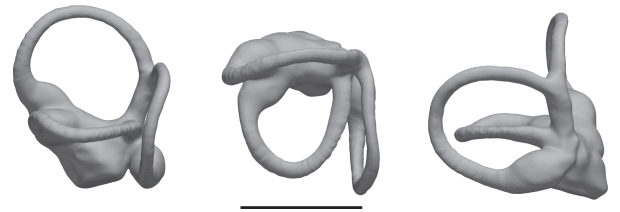
951

952 **Fig. 6.** Reconstructed vestibular shape for the last common ancestor (LCA) of the  
953 main clades of interest as inferred using maximum likelihood methods for  
954 deformation-based 3DGM analyses applied to the hominoid sample under the stem-  
955 hominine phylogenetic hypothesis for dryopiths (Supplementary Fig. 1b), in  
956 posterolateral (left), superior (middle), and posteromedial (right) views. The  
957 reconstructed LCAs depicted are the following: **(a)** crown hominoids; **(b)** crown  
958 hominids; **(c)** crown hominines; **(d)** dryopithecines (*Hispanopithecus* +  
959 *Rudapithecus*). The results for the other phylogenetic hypotheses (not shown) are  
960 virtually identical

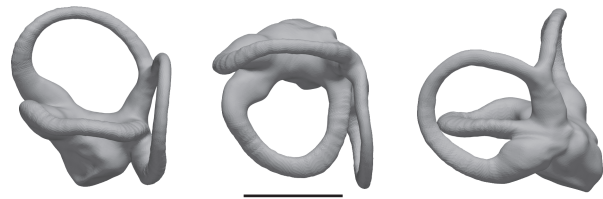
a) *Rudapithecus* RUD 77L



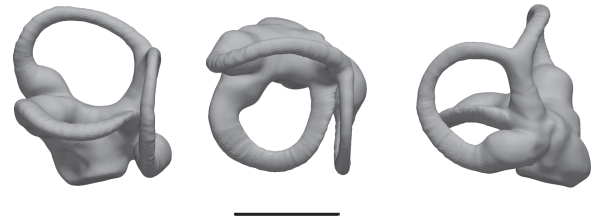
b) *Rudapithecus* RUD 77R



c) *Rudapithecus* RUD 200



d) *Hispanopithecus* IPS18000



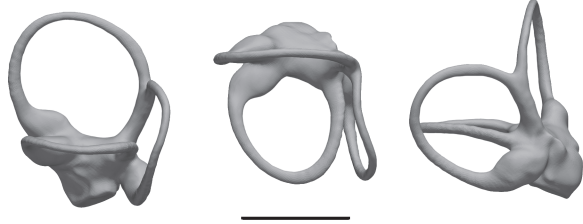
e) *Oreopithecus*



f) *Nacholapithecus*



g) *Hoolock*



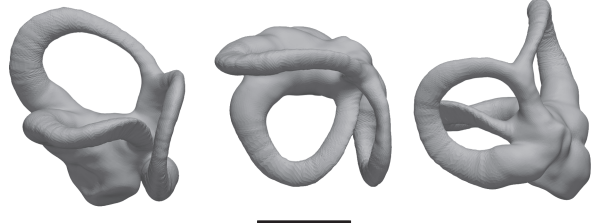
h) *Symphalangus*



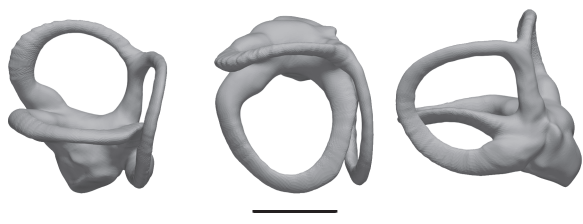
i) *Hylobates*



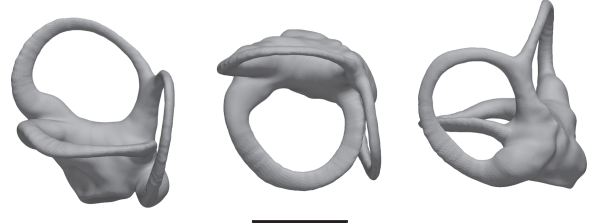
j) *Pongo*



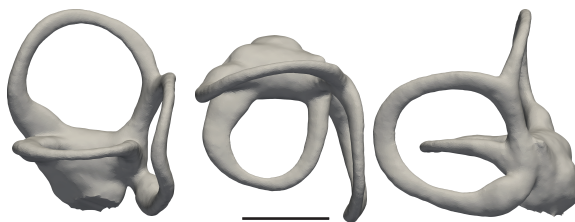
k) *Gorilla*

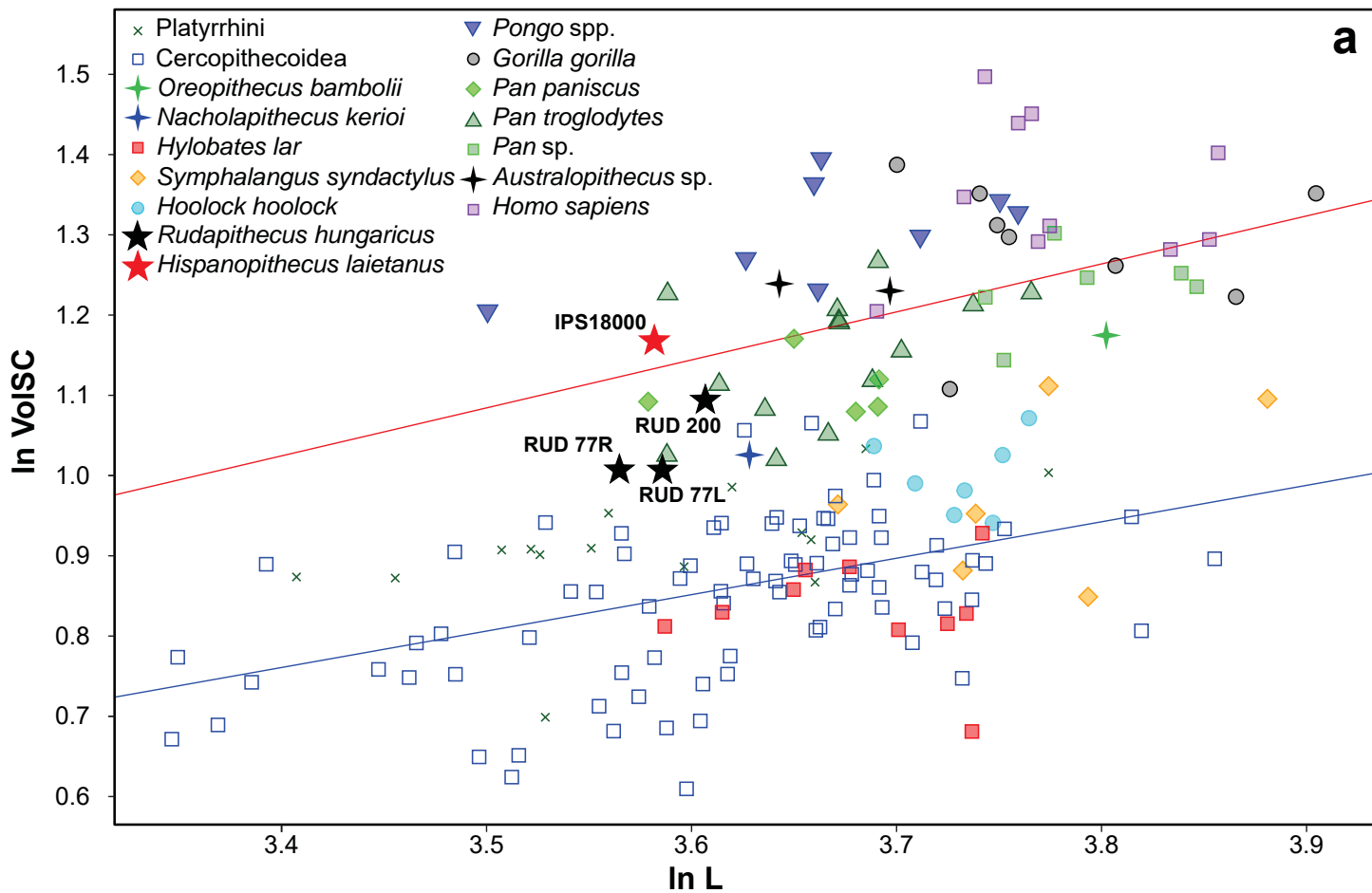


l) *Pan*

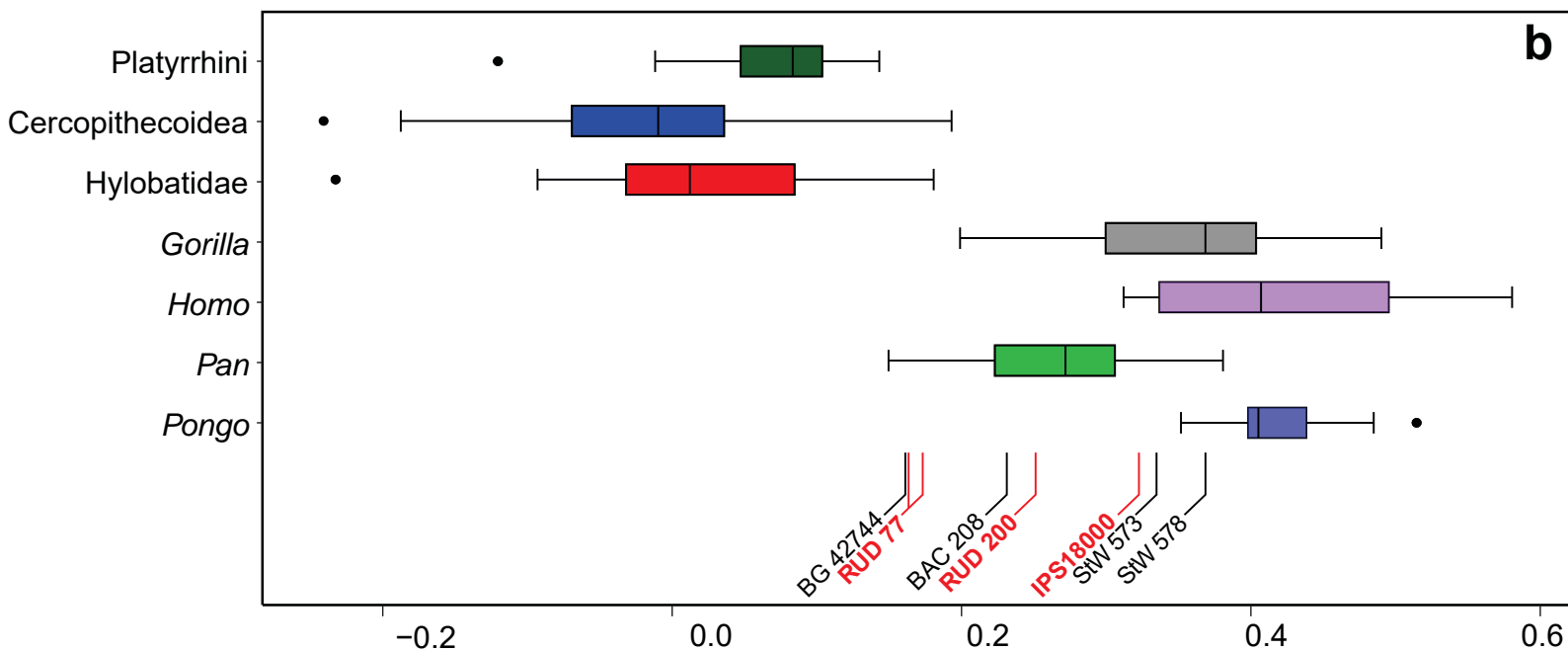


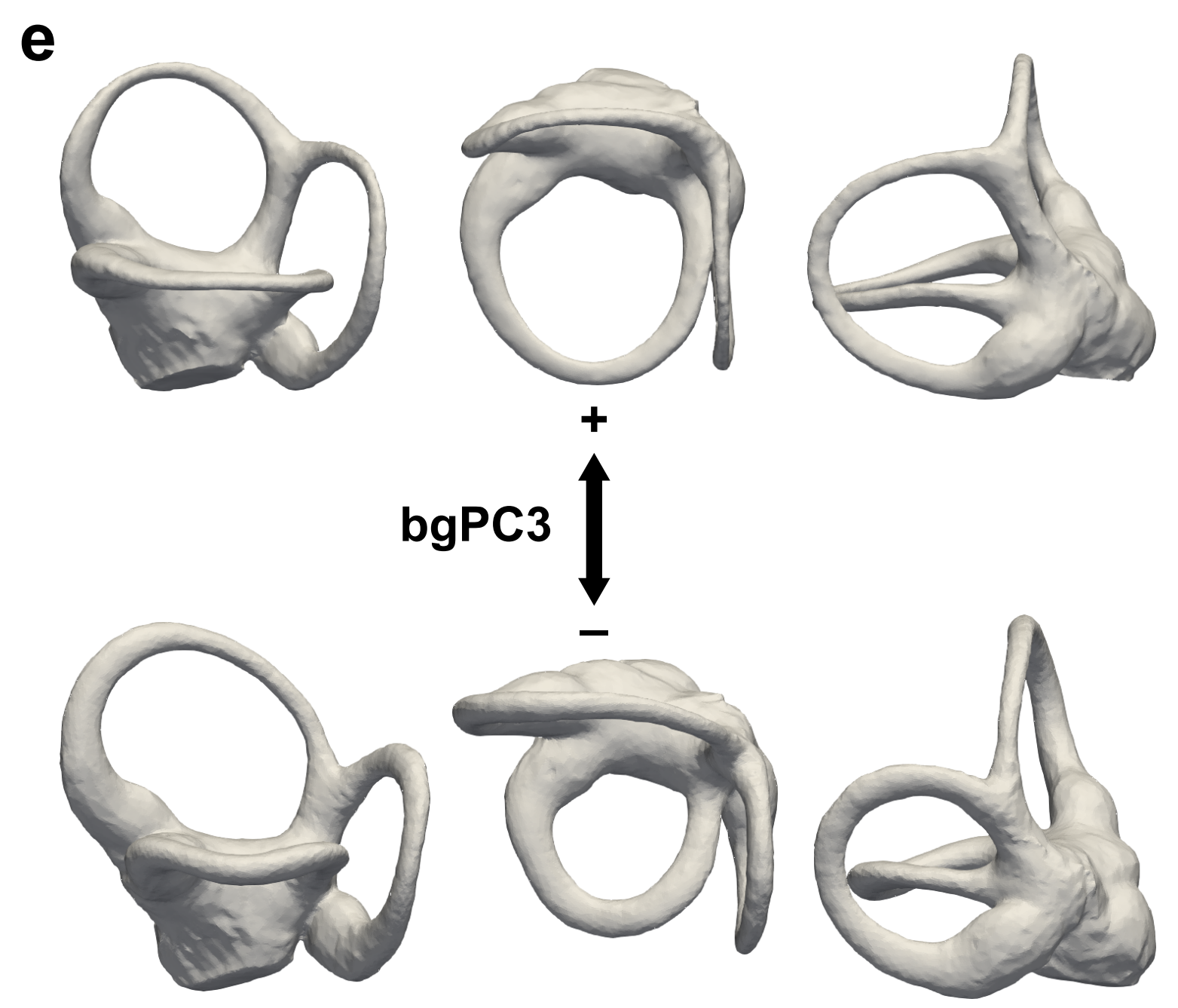
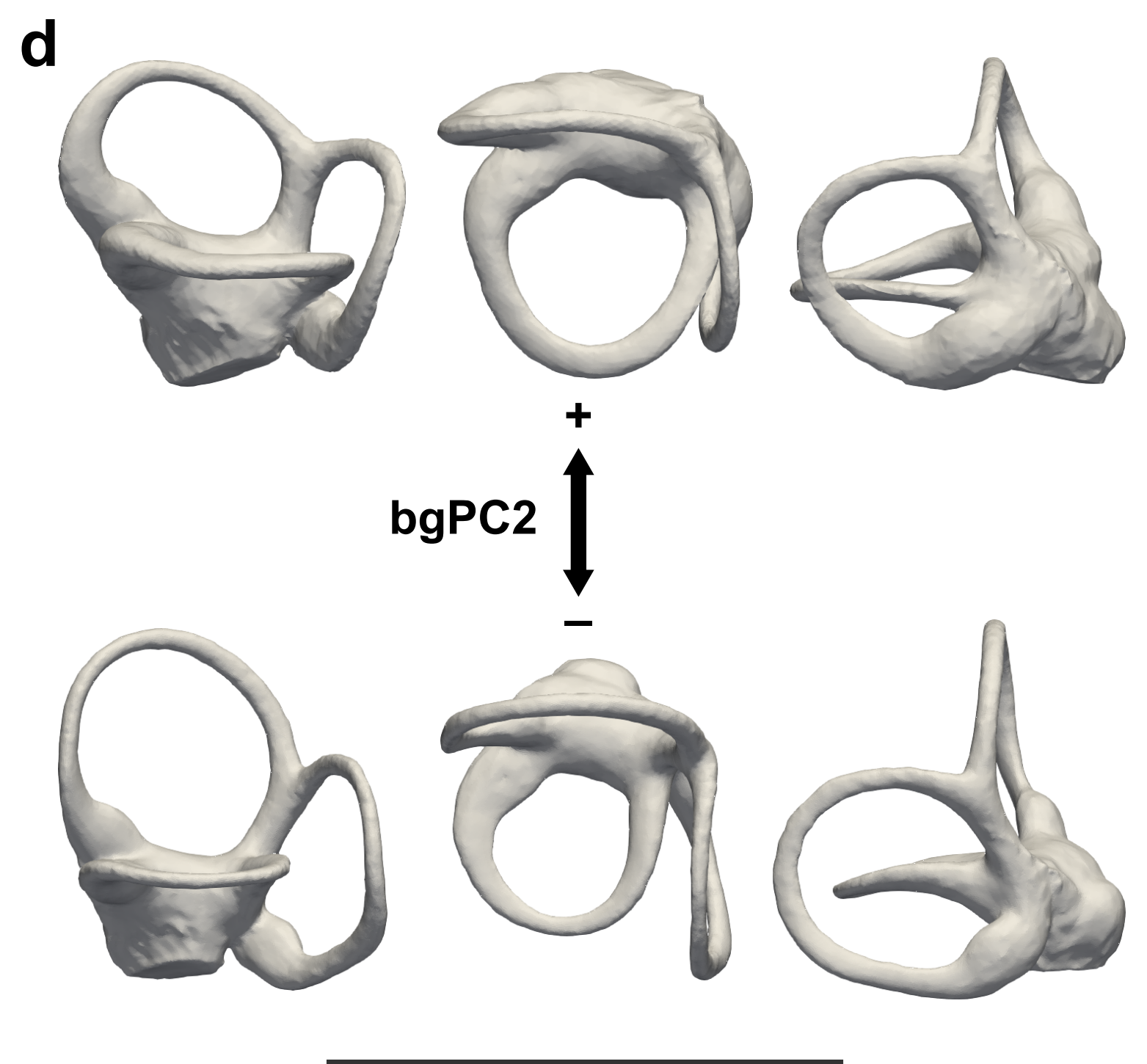
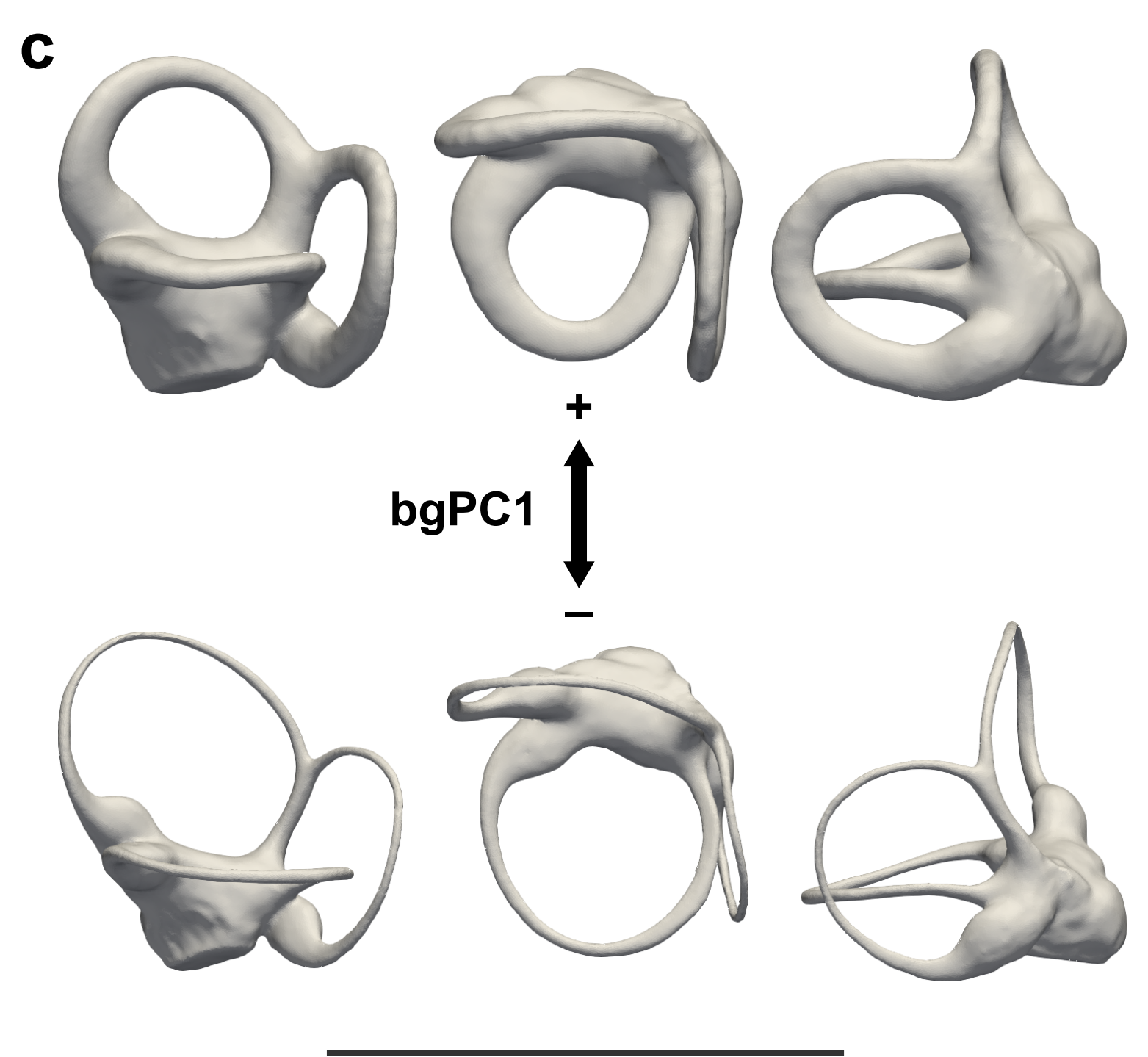
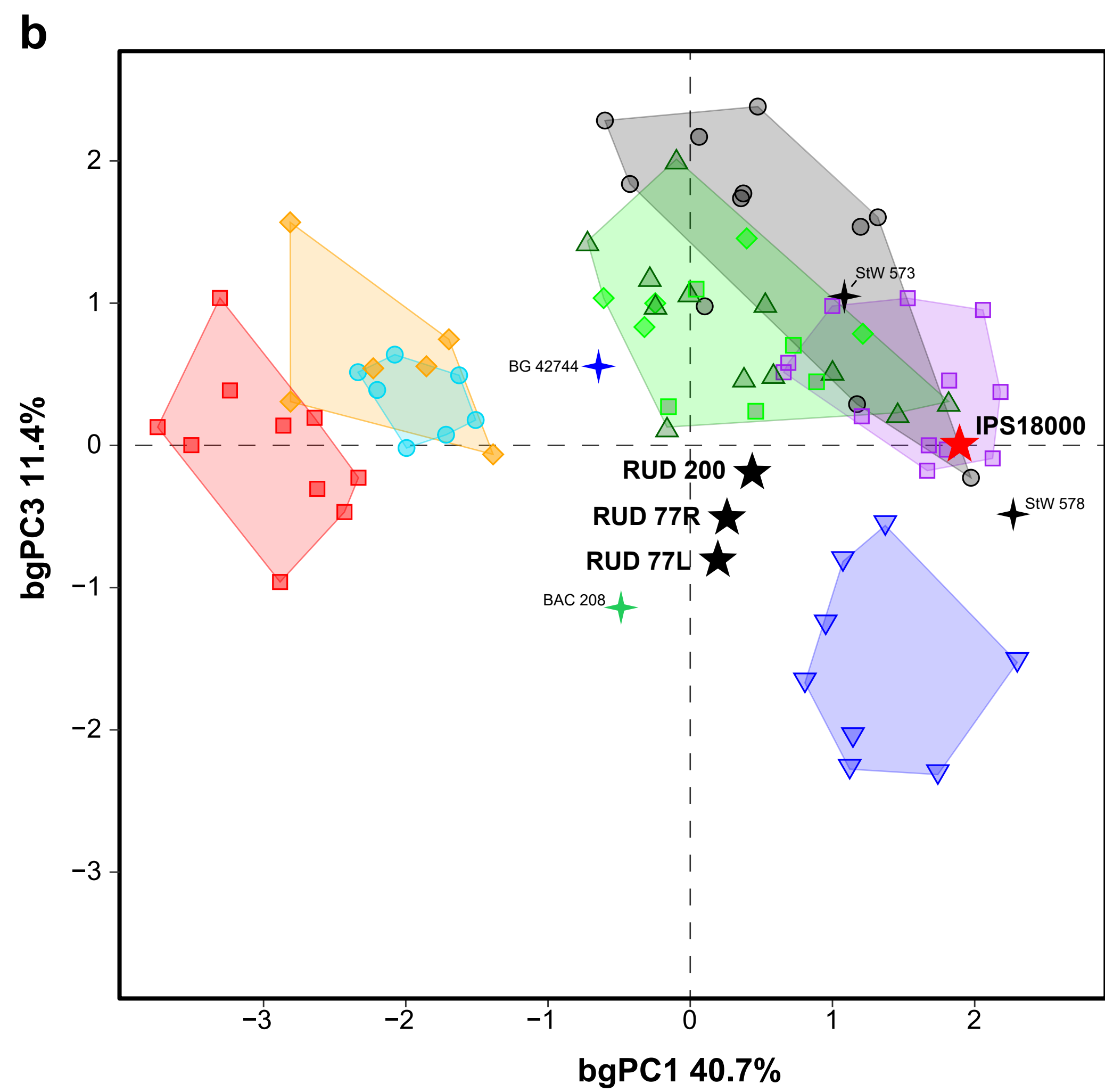
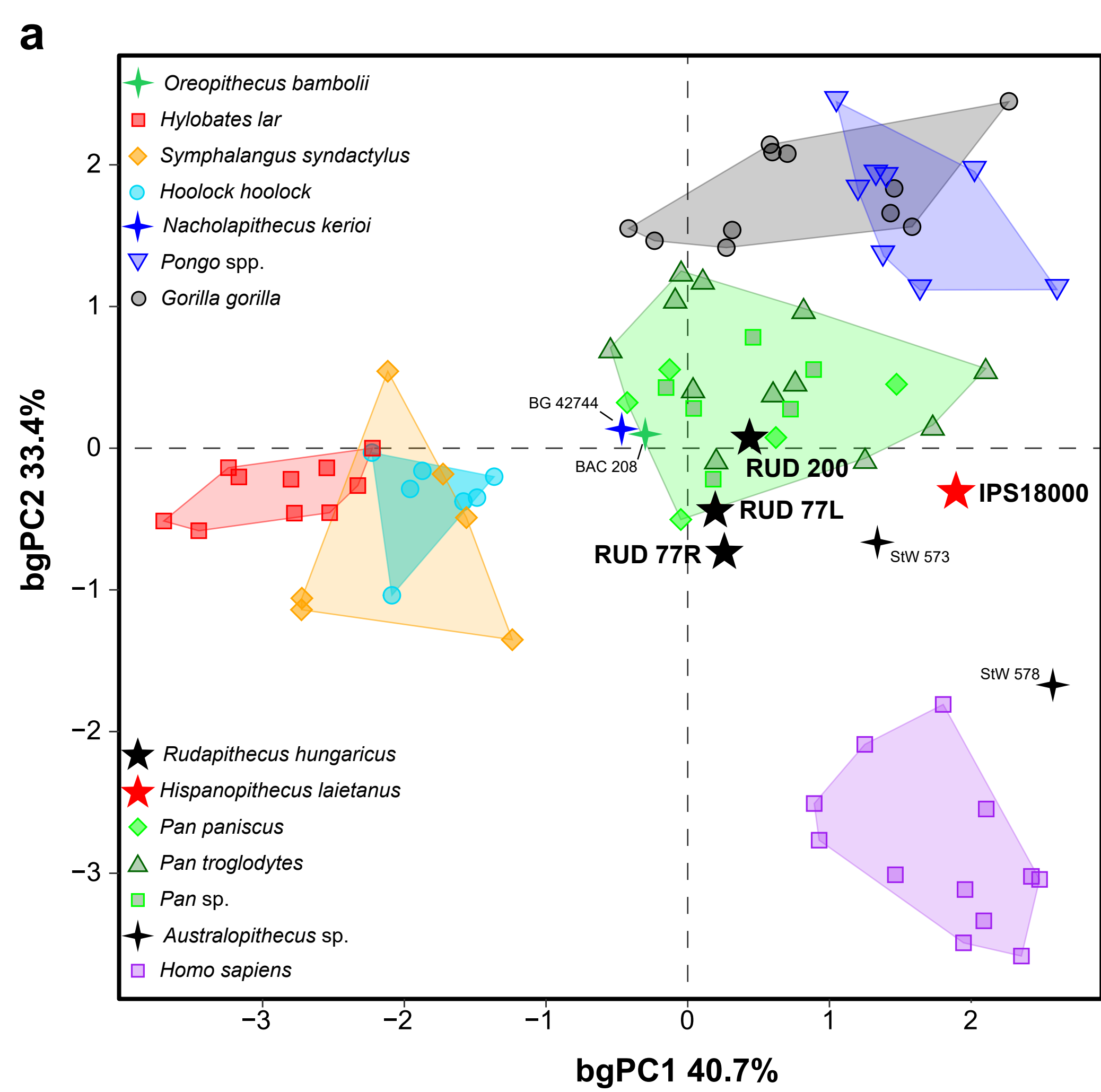
m) *Homo*



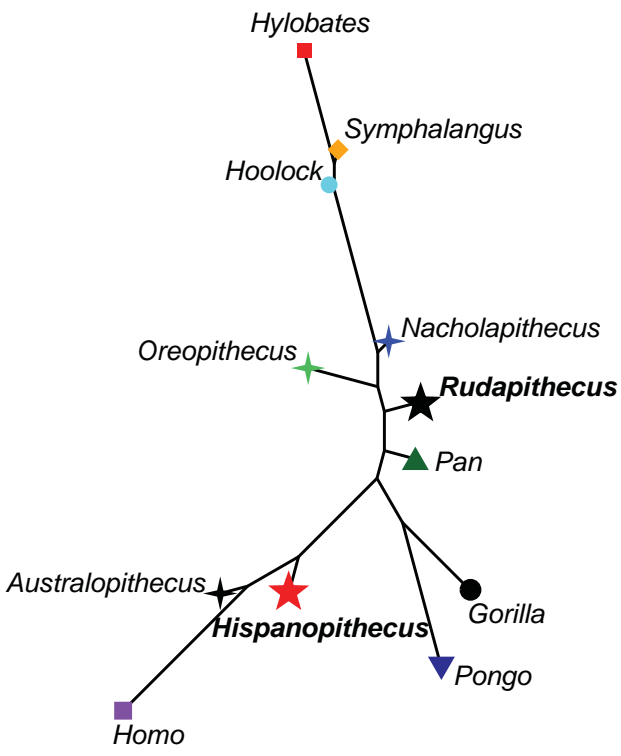


**Allometric residuals**

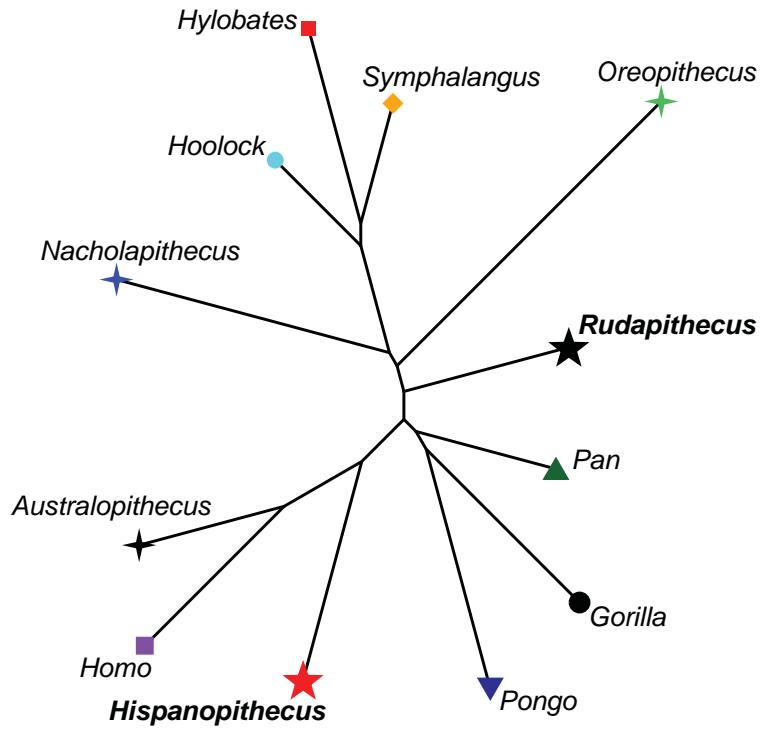


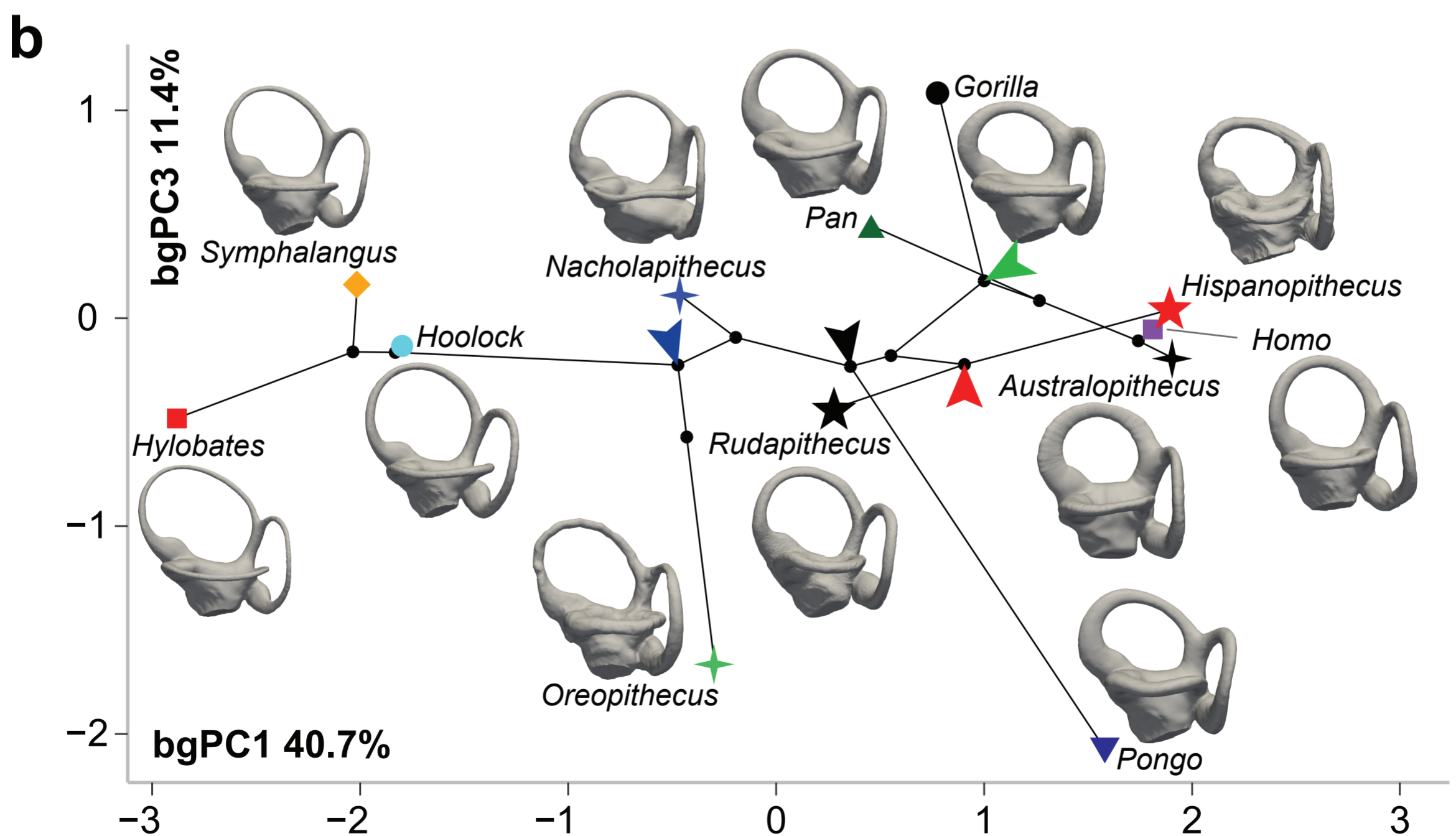
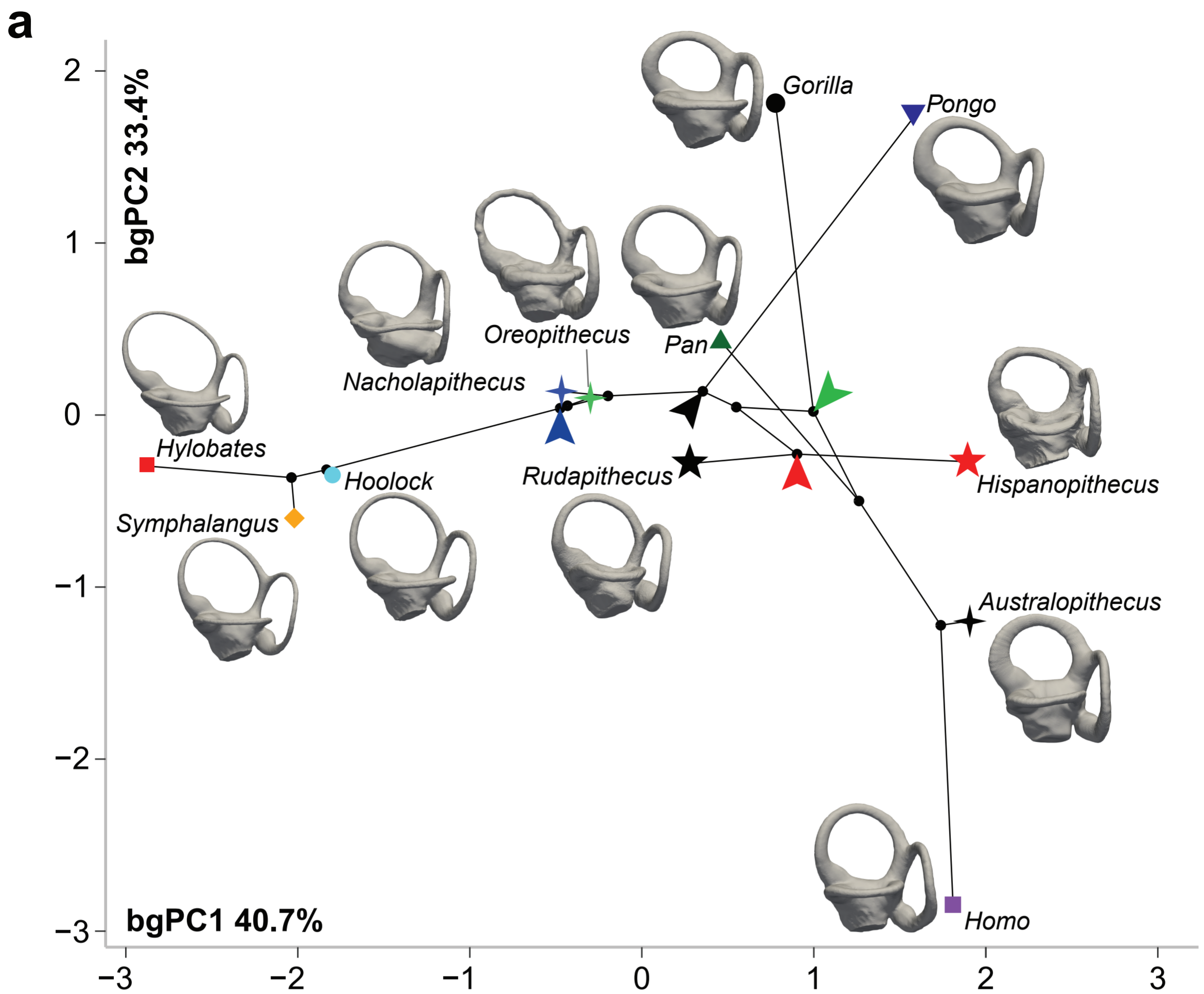


**a**



**b**





▶ Crown hominoid LCA  
 ▶ Crown hominid LCA  
 ▶ Crown hominine LCA  
 ▶ Dryopithecine LCA

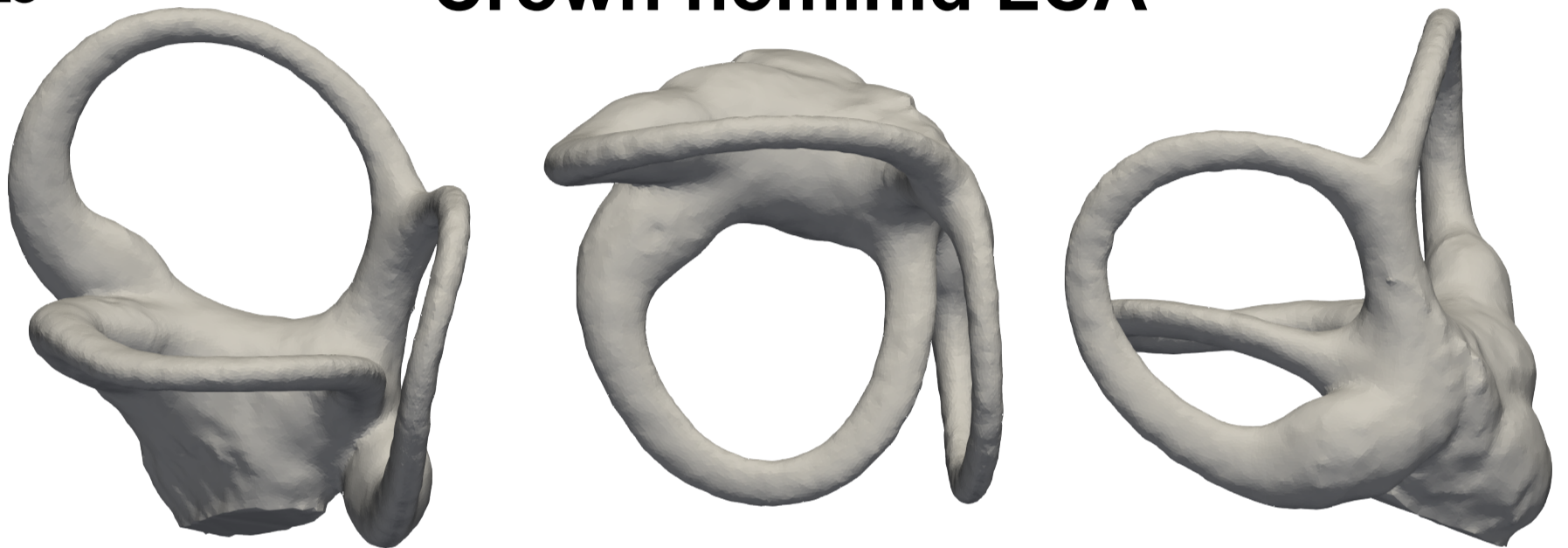
**a**

**Crown hominoid LCA**



**b**

**Crown hominid LCA**



**c**

**Crown hominine LCA**



**d**

**Dryopithecine LCA**







- 1 **Table 2 Mahalanobis distances ( $D^2$ ) between dryopiths and other fossils.** These distances are based on the scores of the
- 2 significant between-group principal components (bgPC1–bgPC3).

| $D^2$   | IPS18000 | RUD 77R | RUD 77L | RUD 200 |
|---|----------|---------|---------|---------|
| IPS18000 ( <i>Hispanopithecus laietanus</i> ) | —        | 2.037   | 2.504   | 1.012   |
| RUD 77R ( <i>Rudapithecus hungaricus</i> )    | 2.037    | —       | 0.179   | 0.772   |
| RUD 77L ( <i>Rudapithecus hungaricus</i> )    | 2.504    | 0.179   | —       | 0.848   |
| RUD 200 ( <i>Rudapithecus hungaricus</i> )    | 1.012    | 0.772   | 0.848   | —       |
| BAC 208 ( <i>Oreopithecus bamboli</i> )       | 6.678    | 2.495   | 1.385   | 3.571   |
| BG 42744 ( <i>Nacholapithecus kerioi</i> )    | 2.286    | 1.270   | 1.505   | 0.416   |
| StW 573 ( <i>Australopithecus</i> sp.)        | 0.703    | 2.587   | 3.657   | 1.637   |
| StW 578 ( <i>Australopithecus</i> sp.)        | 3.080    | 2.745   | 3.087   | 4.479   |

- 3
- 4
- 5